January 2016

On The Design Of Novel Multifunctional Materials By Using Particulate Additives

Ross D. Dunnigan

ON THE DESIGN OF NOVEL MULTIFUNCTIONAL MATERIALS BY USING PARTICULATE ADDITIVES

by

Ross Daniel Dunnigan

Bachelor of Science, University of North Dakota, 2014

A Thesis

Submitted to the Graduate Faculty

of the

University of North Dakota

In partial fulfillment of the requirements

for the degree of

Master of Science

Grand Forks, North Dakota

May

2016

This thesis, submitted by Ross Daniel Dunnigan in partial fulfillment of the requirements for the Degree of Master of Science from the University of North Dakota, has been read by the Faculty Advisory Committee under whom the work has been done and is hereby approved.

Surojit Gupta, Ph.D.

Matthew Cavalli, Ph.D., P.E.

Clemen Tang, Ph.D.

This thesis is being submitted by the appointed advisory committee as having met all of the requirements of the Graduate School at the University of North Dakota and is hereby approved.

Wayne Swisher, Ph.D.
Dean of the School of Graduate Studies

May 4, 2016

Date

PERMISSION

Title	ON THE DESIGN OF NOVEL MULTIFUNCTIONAL MATERIALS BY USING PARTICULATE ADDITIVES
Department	Mechanical Engineering
Degree	Master of Science

In presenting this thesis in partial fulfillment of the requirements for a graduate degree from the University of North Dakota, I agree that the library of this University shall make it freely available for inspection. I further agree that permission for extensive copying for scholarly purposes may be granted by the professor who supervised my thesis work or, in his absence, by the Chairperson of the department or the Dean of the Graduate School. It is understood that any copying or publication or other use of this thesis or part thereof for financial gain shall not be allowed without my written permission. It is also understood that due recognition shall be given to me and the University of North Dakota in any scholarly use which may be made of any material in my thesis.

Ross Daniel Dunnigan

May 5, 2016

TABLE OF CONTENTS

LIST OF FIGURES

ACKNOWLEDGEMENTS

I am grateful to my colleagues, Sujan Ghosh, and Faisal Riyad, for without them this work would not have been possible. I would like to express my sincerest gratitude to Dr. Surojit Gupta at the University of North Dakota for all of the aid and support I received during my studies.

In addition, I would like to thank Thomas Hammann for his previous work and my family, fiancé, and her family for always being there for me.

ABSTRACT

This thesis has been organized into five chapters. The main focus of this thesis is to design novel multifunctional materials by using particulate additives. Chapter 1 is devoted to reviewing recent studies in additive manufacturing (AM) and other background information. In Chapter 2, the synthesis and characterization of novel Ti_3SiC_2-reinforced Zn-matrix composites is reported. During this study, all the Zn composites were hot pressed at 500°C for 5 min at a uniaxial pressure of ~150 MPa. Microstructure analysis by SEM (Scanning Electron Microscopy) and phase analysis by XRD (X-ray Diffraction) confirmed that there was minimal interfacial reaction between Ti_3SiC_2 particles and the Zn matrix. The addition of Ti_3SiC_2 improved the tribological performance of these composites against alumina substrates but did not have any beneficial effect on the mechanical performance. The addition of Ti_3SiC_2 particulates to metal and polymer matrices show interesting properties. Chapter 3 will focus on additive manufacturing of Ti_3SiC_2 particulates in a polymer matrix. Waste materials are a big problem in the world. Chapters 4 and 5 focus on recycling materials. The mechanical and tribological properties of the Resin-Nylon and Resin-Polyester composites are reported, respectively.

CHAPTER I

INTRODUCTION

1.1 Types of Additive Manufacturing

Additive Manufacturing (AM) is also known as 3D printing. Recently, 3D printing has become very important in the modern world. This is because there are so many different materials that can now be 3D printed. Metals, polymers, ceramics, and even human tissue are some of the printable materials. This opens up many applications for 3D printing and allows humanity to create complex objects for new futuristic designs.

Rapid Prototyping was the first form of AM using computer-aided design (CAD) [1]. This form of AM was created in the 1980s to help engineers have a realization of what they had in mind [1]. This new manufacturing method saved money, time, labor, and was able to create complex designs that would be very difficult to machine [1]. Rapid Prototyping also allows for flexibility in design. Figure 1.1 is a diagram on the processes that need to occur to create a 3D printed object. The first step is to think of a design and create the design on a CAD program. After the design is created, an analysis of the design is performed to ensure the design can handle the desired loads. Assuming everything works out with the design, the file is then saved as a STL file. This file takes the model and cuts it into thin layers so it can be created by the desired 3D printer. After printing, the model is cleaned of excess material and is tested to ensure that it works as designed. If it does not work, the process should be repeated again from the beginning.

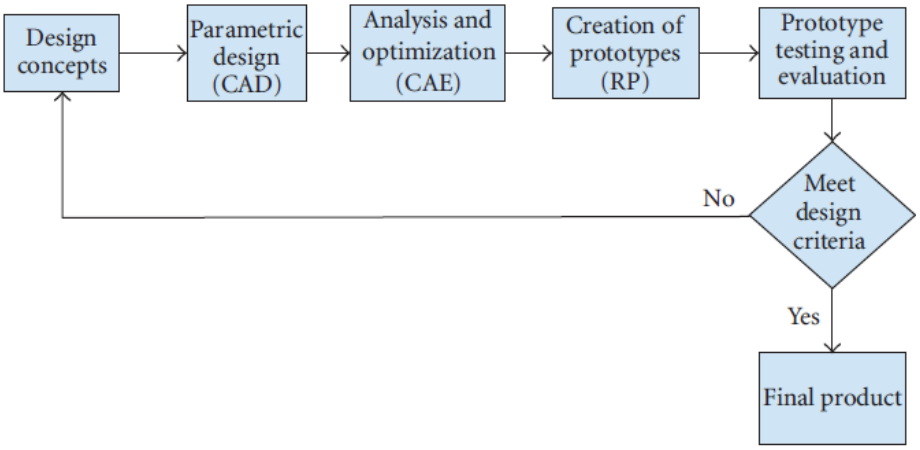

Figure 1.1: A typical product development cycle [2]

Figure 1.2 shows a diagram of many different AM processes. The AM processes listed in the diagram are Fused Deposition Modeling (FDM), Stereolithography (SL), Polyjet, Laminated Object Manufacturing (LOM), Selective Laser Sintering (SLS), Electron Beam Melting (EBM), Laser Engineered Net Shaping (LENS), 3DP and Prometal.

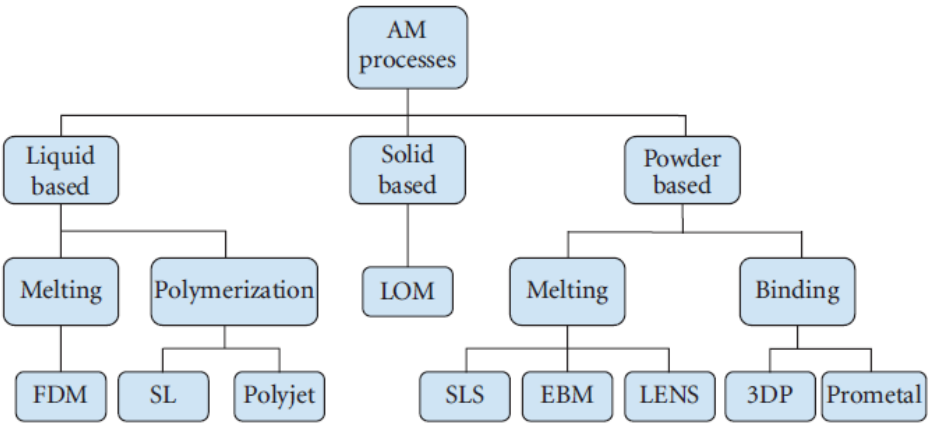

Figure 1.2: Different types of three-dimensional printing processes [3]

Fused Deposition Modeling (FDM) uses polymers in the form of a thin filament. This filament is fed into an extrusion tip which is then heated until the filament becomes malleable. The filament is then deposited onto the build platform to create the model. "The inherent advantages of FDM printing are, (a) there is no chemical post-processing required, (b) no resin to

cure, (c) less expensive machine, and (d) it is more cost-effective" [1]. However, the main disadvantage of FDM is that the z-axis resolution is low and a finishing process may be required [1]. Stereolithography (SL) uses a photosensitive polymer that is cured by a UV laser. The printer creates models faster compared to FDM but has some disadvantages. For example, (a) over-curing can occur because there is no fusing involved with the bottom layer of overhanging parts [1], and (b) the resin used is in the liquid form can cause an error with border position control [1]. Polyjet uses inkjet technologies to create models. The model is printed in the x- and y-axis and then cured with UV light. After the curing is complete the model then has another layer printed on top of the previous layer. The models from this printer have high resolutions, but the models are weaker compared to other printing methods.

Laminated Object Manufacturing (LOM) uses both AM and subtractive techniques to print layer by layer. The layers are made individually and then the layers are put on top of one another and are bonded together by heat, pressure, and thermal adhesive coating [1]. This is a low-cost process with no post-processing and with no need for support structures [1]. There also is no deformation or phase change during the process [1]. However, this process is time-consuming, has low surface definition, and the material is directionally dependent which can cause it to be weak in certain directions [1].

Selective Laser Sintering (SLS) uses a powder to print. The particles sit in a container on top of a piston. From here the powder is heated nearly to its melting point, then a carbon dioxide laser is used to fuse the powders together creating a thin layer [1]. The piston is then lowered, where a new layer is created on top of the existing layer until the model is complete [1]. The advantages of SLS are the wide range of materials that can be used with this method and unused

powder can be reused [1]. Unfortunately, the accuracy of this printer is limited to the particle size of the material and some materials need to be printed in an inert environment [1].

There are numerous methods for fabricating metallic samples. Electron Beam Melting (EBM) uses a high powered voltage in the form of an electron laser beam to melt powders. To avoid oxidation, the process is done in a vacuum chamber which makes this printing method ideal for future space exhibitions [1]. Laser Engineered Net Shaping (LENS) melts a metal powder using a high-powered laser beam until it becomes molten [1]. The material solidifies from cooling and it is created in an atmosphere of Argon [1]. One problem with this process is the possibility of residual stresses being created because of uneven heating or cooling processes [1]. 3DP uses a water-based liquid binder in a jet that binds a starch-based powder together to create the model [1]. Prometal uses a stainless steel powder where a liquid binder is spurt out of jets to create a layer of stainless steel. The powder is in a container that is lifted and lowered by a piston [1]. The piston lowers every time a new layer is created until the final object is created. However, after the object is made, sintering, infiltration, and finishing processes are required [1].

In this thesis, I will mainly focus on SL for fabricating Polymer Matrix Composites (PMCs). In addition, I will also explore Hot Pressing (HP) for fabricating MRMs (MAX Reinforced Metals).

1.2 MAX Phases

MAX phases have many extraordinary properties and act as both metals and ceramics. They have metallic properties such as high electrical and thermal conductivity and ceramic properties that show great resistance to oxidation and thermal shock [4]. MAX phases also contain natural nanolaminates which causes them to be highly machinable and to have a low coefficient

of friction [4]. Along with having many great properties, MAX phases can be made up of many different elements. Figure 1.3 shows the possible elements that can be used to create a MAX phase. MAX is an acronym, where M is an early transition metal, A is a group A element, and X is Carbon and/or Nitrogen.

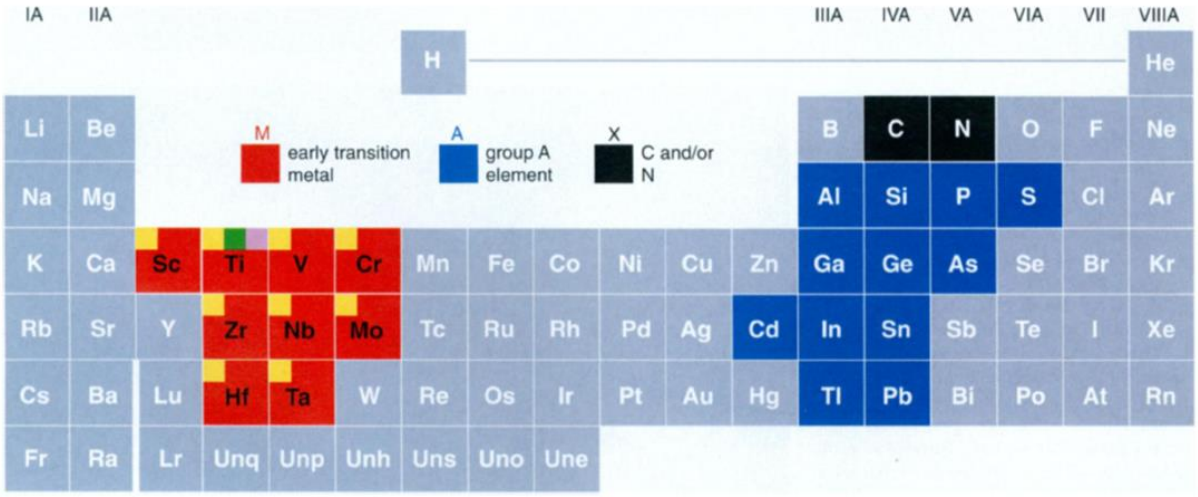

Figure 1.3: Different elements which form MAX Phases in a periodic table [5]

MAX phases consist of over 60 ternary carbides and nitrides. This is because the chemical formula is $M_{n+1}AX_n$, where n can be anywhere from 1-3. Figure 1.4 shows the unit cells of MAX phases depending on whether n is 1, 2, or 3. The colors in the unit cells represent the placement of the elements within the unit cell. The red spheres (M) are an early transition metal, the blue spheres (A) are a group A element, and the black spheres (X) are Carbon or Nitrogen. The unit cells of the MAX phases are characterized by the near close-packed M layers interleaved with layers of pure group A-element, with the X-atoms filling the octahedral sites between the former [4].

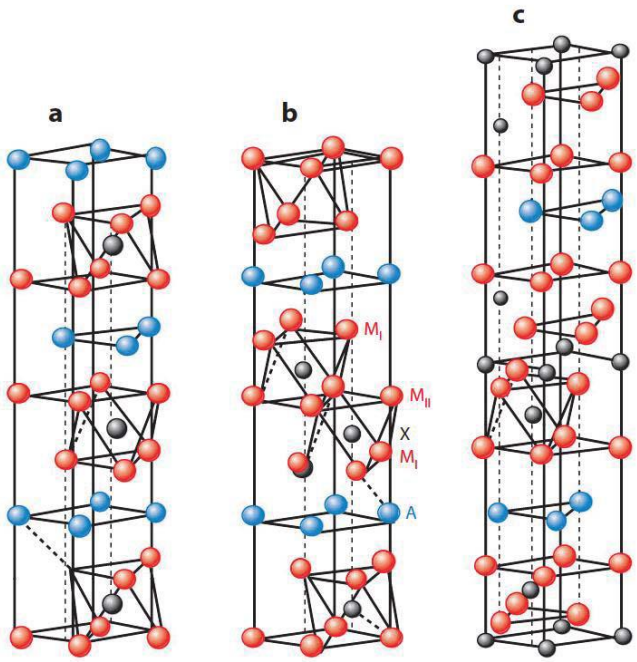

Figure 1.4: Unit cells of MAX phases: (a) M_2AX (211), (b) M_3AX_2 (312), and (c) M_4AX_3 (413) [6].

In this thesis, Ti_3SiC_2 will be used as a particulate additive in designing different types of PMCs as Ti_3SiC_2 is one of the most studied MAX phases because of its extraordinary properties [4].

1.3 3D Printing of Ti_3SiC_2

Recently, Ti_3SiC_2 powders were 3D printed by using a Z402 3D printing system (Z-Corp) [7]. The Z402 printer has a feed bay, a build bay, and a binder spray head. The printing process consists of the binder spray head spraying onto the first layer of the powder. Once the layer has been sprayed, a new layer of powder is released from the feed bay into the build bay. The binder spray head is then used to bind the powder of the new layer. This process is repeated until the sample is created. The samples are then Cold Isostatically Pressed (CIP) by applying a pressure

of 379 MPa for 15 minutes. The cold pressed samples were then sintered at 1600°C for 4 hours. Figure 1.5 illustrates the fabrication process of the Ti_3SiC_2 composites.

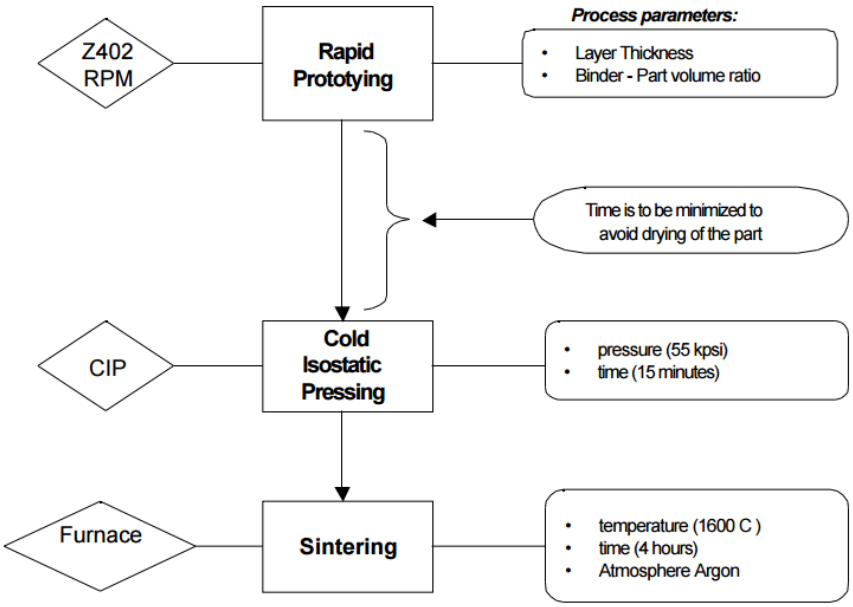

Figure 1.5: 3D fabrication process for fabricating structures by using Ti_3SiC_2 [7]

Figure 1.6 compares the effect of binder concentration and CIP on the densities of the samples. Clearly, the porosity decreased when a cold isostatic press was used on the samples. More importantly, this research study proved that Ti_3SiC_2 can be 3D printed.

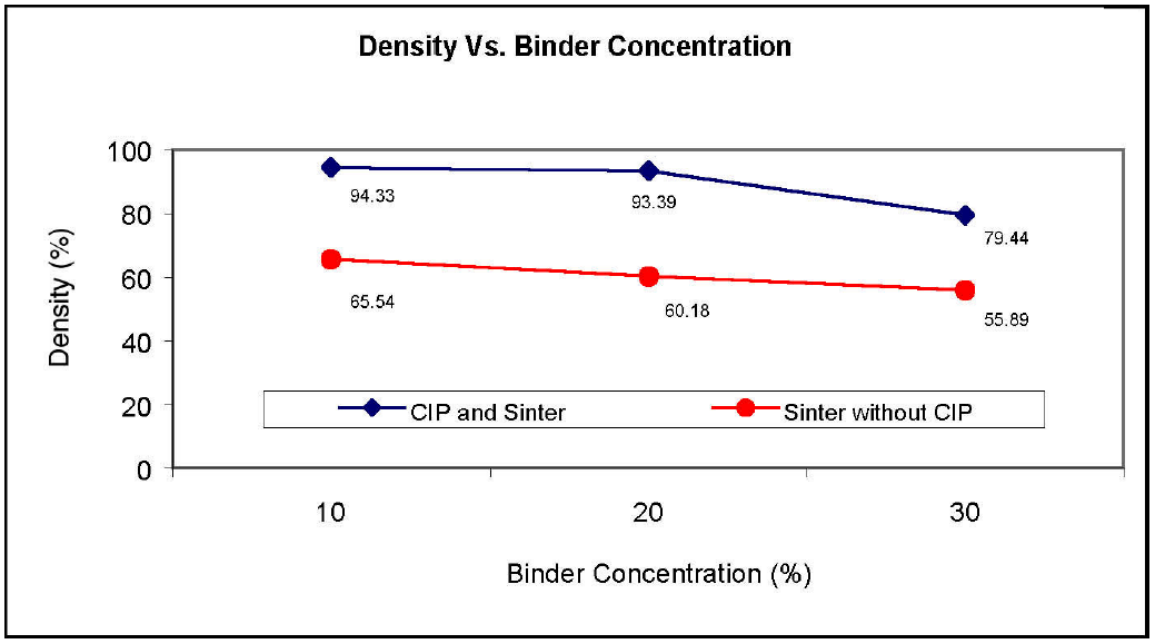

Figure 1.6: Plot of density variation vs. different processes and processing parameters [7]

1.4 Background Information on Form 1+ 3D printer

The Form 1+ (Formlabs Inc., Somerville, MA) is a high resolution SL 3D printer. Figure 1.7 shows the printer. The platform lowers into the resin where UV light is used to cure the resin. Figure 1.8 shows the lower limit of resin in the 3D printer. Once the resin is above the designated limit, the printer can print the required object.

Figure 1.7: A typical Form 1+ printer

Figure 1.8: An indicator mark showing minimum threshold level in a 3D printer

Initially, the drawing of the engineering component is saved as a STL file. The STL file is then uploaded in the PreForm program, which is included with the Form 1+ printer. Figure 1.9 shows the snapshot of the program. Different layer thicknesses can be selected by using the program. In this thesis, a resolution of 0.2 mm was used for printing the samples.

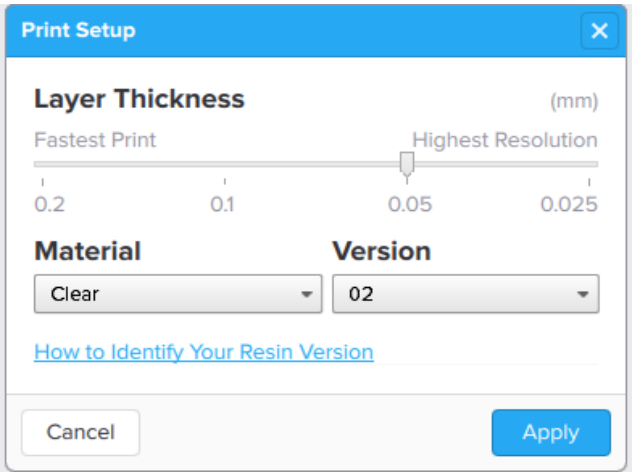

Figure 1.9: Print setup before importing a model

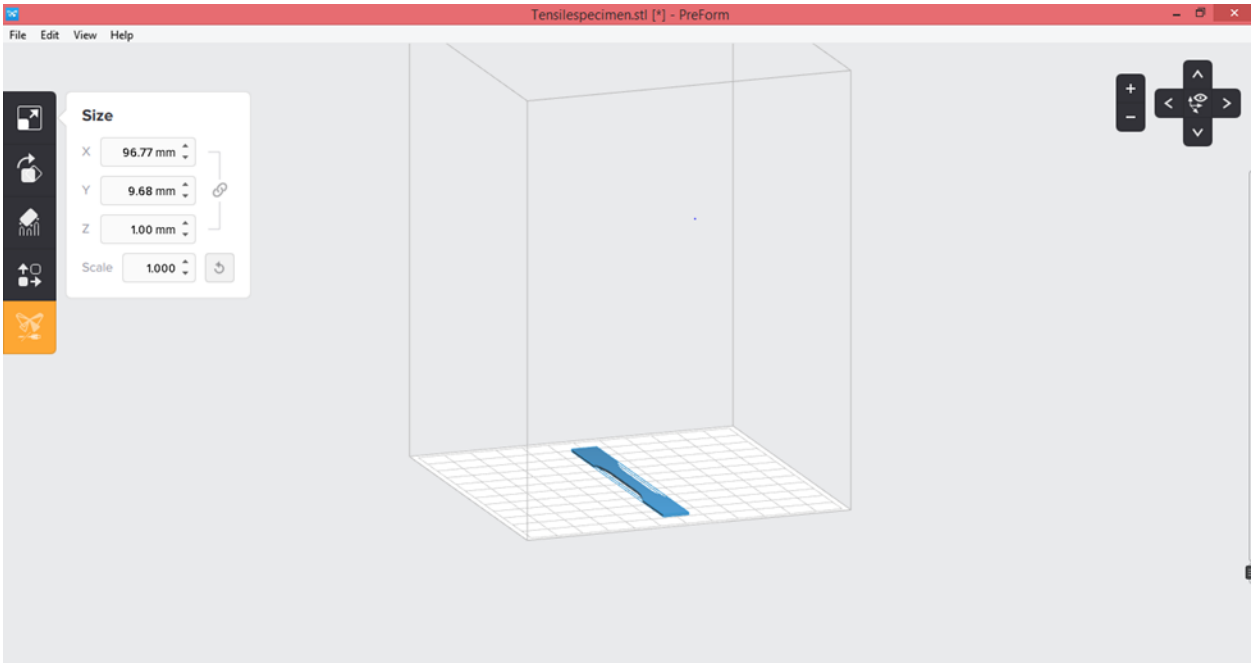

Figure 1.10: A snapshot of the main screen of the PreForm software

Figure 1.10 shows a schematic of a tensile specimen on the build platform. Figure 1.11 shows an example of a printed sample. The sample was then scraped off by using a spatula. The final product is immersed and shaken in 96-98% ethyl alcohol for 10 minutes. The sample is then left out to dry and is ready for use.

Figure 1.11: A picture of the hopper 3D printed by Form 1 lab

CHAPTER II

SYNTHESIS AND CHARACTERIZATION OF Ti_3SiC_2 PARTICULATES REINFORCED NOVEL Zn MATRIX COMPOSITES

2.1 Introduction

This work has been published in the *Journal of Materials Engineering and Performance*. Zn-based alloys (ZA) can perform better than bronze, cast iron, and aluminum alloys for many different engineering and tribological applications [1-6]. Zn is a softer metal which allows for an excellent castability. ZA not only show great castability but also show good wear-resistance and mechanical strength. Researchers have been reinforcing Zn with ceramic particulates to enhance the mechanical and tribological properties of Zn. The additive hard phases include but are not limited to TiO_2 [1], Al_2O_3 short fiber [2], garnet [3], glass fibers [4], and SiC [5, 6]. The addition of MAX phases will be an important study both scientifically and technologically to see how the mechanical and tribological behavior is affected for the Zn matrix.

Promising properties have been seen from metal composite MAX phases (MAXMET's) [7-15]. An electro-friction material has been discovered from Cu/Ti_3SiC_2 composites [7]. Solid-lubrication behaviors have been seen when Ag was added to MAX phase composites over a wide range of temperatures [10,11]. Mg in MAX phases have shown many magnificent properties such as an ultrahigh damping, being readily machinable, relatively stiff, along with being strong and light [10]. A yield strength twice the amount of pure Al has been seen when 40 vol% Ti_3AlC_2 particulates was added to an Al matrix [11]. A 1.5 times higher specific compressive strength was seen with an Aluminum alloy/Ti_2AlC composite than the specific yield strength of the peak-aged aluminum alloy [12]. A higher damping with a stress up to 200 MPa was shown with a

Ti_3SiC_2 -NiTi alloy composite [13]. This is the best damping seen in a MAXMET composite [13]. The mechanical performance of Al and Sn was enhanced by the addition of Ti_3SiC_2 particulates [14,15]. The mechanical and tribological behavior of Zn based MRM (Metal Reinforced with MAX) composites will be discussed in this thesis.

2.2 Experimental

Calculated concentrations of Ti_3SiC_2 powder (-325 mesh, Kanthal, Hallstahammar, Sweden) and Zn powder (-100 mesh, Alfa Aesar, Ward Hill, MA) were dry ball milled (8000 M mixer Mill, SPEX SamplePrep, Metuchen, NJ) for 2 minutes. The powders were poured into a die (EQ-Die-12D, MTI Corporation, Richmond, CA) where they were sintered in ambient air by hot pressing them with a uniaxial compressive stress of approximately 150 MPa at 500^oC for 5 minutes. The composites cooled to room temperature inside the hot press before being removed. The Zn based MRM composites were fabricated using 5 vol% (Zn(95)-Ti_3SiC_2(5)), 10 vol% (Zn(90)-Ti_3SiC_2(10)), 20 vol% (Zn(80)-Ti_3SiC_2(20)), and 30 vol% (Zn(70)-Ti_3SiC_2(30)) Ti_3SiC_2 particulates with a pure Zn sample for comparison.

The rule of mixtures was used to calculate the theoretical density of the Ti_3SiC_2 and Zn phases. The mass and dimensions of each sample were measured and the experimental density was then discovered. Using the experimental and theoretical density, the relative density was able to be calculated. Each composite was then machined into approximately 3 mm cubes for mechanical testing. A mechanical tester (Shimadzu AD-IS UTM, Shimadzu Scientific Instruments Inc., Columbia, MD) was used for compression testing. A deflection rate of 1 mm/min was used on a set of 3 samples for each composition. Plots were made for stress verse displacement. However, experimental limitations caused an inaccurate measurement for strain during the mechanical

testing. When the stress versus displacement plot transitions from a linear curve to a non-linear curve, defined as the critical stress, it will be called the yield strength in this thesis. A regression of R^2 >0.95 was used for the linear region of the composites. The 3 yield strength measurement averages are reported in this thesis. All of the composites were tested using a Vicker's micro-hardness indentor (Mitutoyo HM-112, Mitutoyo Corporation, Aurora, IL). Before the hardness testing occurred, the composites were polished to (R_a < 1µm). The samples had a force of 9.8 N applied to them for 15 s. An average of 5 readings were used for each composite and are reported in this thesis.

A Bruker Microdiffartomoeter was used for the X-ray diffraction measurements. A CSM Tribometer (CSM Instruments SA, Peseux, Switzerland) with a tab-on-disk, 50 cm/s linear speed, 1000 m sliding distance, and a ~9 mm track radius was used to determine the tribology measurements. Before the testing could begin tabs were machined with dimensions of ~4 mm x ~ 4 mm x ~3 mm and polished to a ~1 µm finish. To ensure that all the samples had a R_a <1 µm a surface proflometer (Surfcom 480A, Tokyo Seimitsu Co. Ltd., Japan) was used. There were three experimental studies completed for each composition. For a single experiment, the mean response was calculated by using the average of all the friction coefficient (µ) readings, which is shown as μ_{mean} in the text. The samples and substrates mass were measured with a weighing scale (Model AL204, Mettler Toledo, Columbus, OH) before and after testing. The specific wear rate (WR) was calculated from:

$$WR = (m_i - m_f)/(\rho * N * d) \quad (2.1)$$

where, m_i is the initial mass, m_f is the final mass, ρ is density of the composite, N is the applied load, and d is the total distance traversed by the tab during the tribology testing.

Au/Pd was the coating used for the Alumina samples which were coated using a Balzers SCD 030 sputter-coater (BAL-TEC RMC, Tucson AZ USA) which were then mounted on aluminum mounts. Secondary Electron (SE) images and Backscattered Electron (BSE) images were performed on all of the samples by using a JEOL JSM-6490LV Scanning Electron Microscope (JEOL USA, Inc., Peabody, Massachusetts). A Thermo Nanotrace Energy Dispersive X-ray detector with a NSS-300e acquisition engine was used for the X-Ray information. The measuring of the Carbon (C) had a quite low accuracy in the EDS. This means that all of the compositions listed could possibly contain C, especially the substoichimetric oxides. $\{C_x\}$ will be used to show the presence of C in the tribofilms within the composition.

2.3 Microstructure and Phase Analysis

SE images of different MRM composites are shown in Figure 2.1. These images show that Ti_3SiC_2 particulates are well-dispersed inside the Zn matrix.

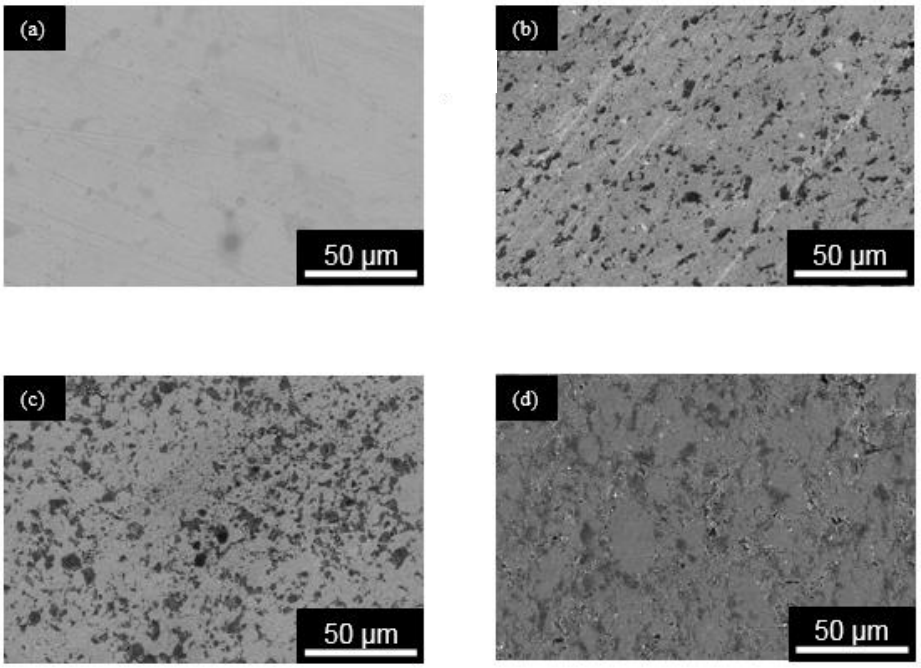

Figure 2.1: SE micrographs of Zn-312Si (a) pure Zn (b) Zn-10%312Si (c) Zn-20%312Si (d), Zn-30%312Si

An XRD plot can be seen in Figure 2.2 for Zn-based MRM composites. The XRD shows that negligible reaction occurred between the Zn and Ti_3SiC_2 particulates.

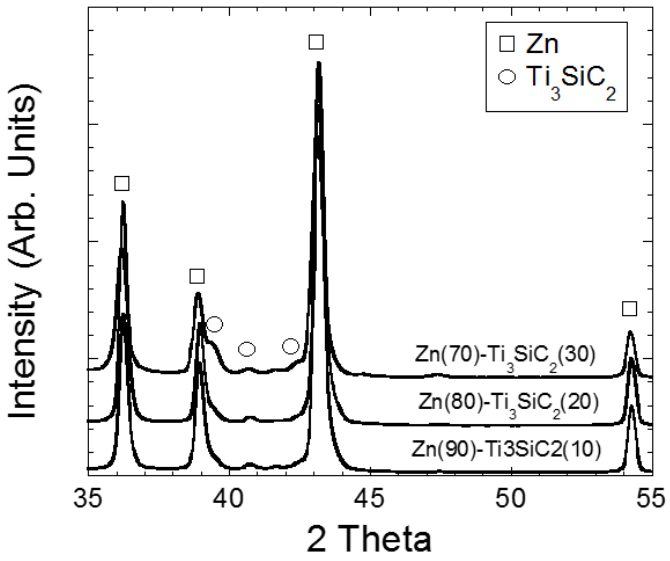

Figure 2.2: XRD profiles of different composites of Zn-Ti_3SiC_2

The porosity of the composites with Ti_3SiC_2 additions, shown on the x-axis, are in Figure 2.3. As the addition of Ti_3SiC_2 concentrations become higher the samples become more difficult to make dense. Al [14] and Sn [15] based MRM composites showed similar results as a higher vol% of Ti_3SiC_2 was added to the matrices.

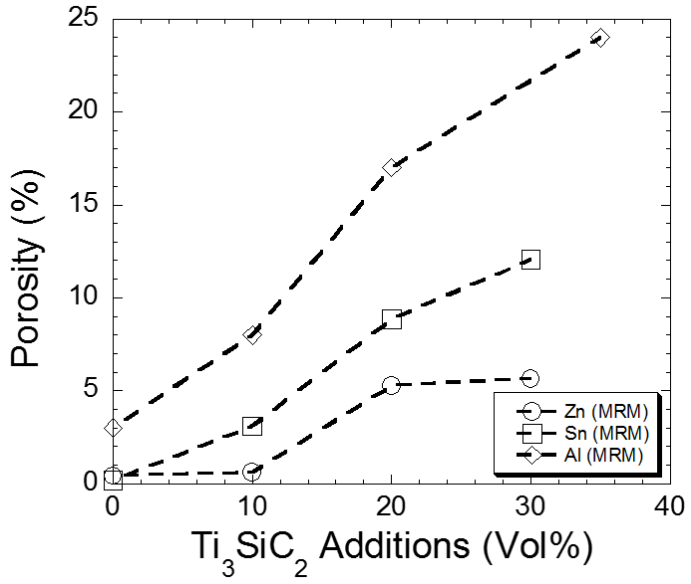

Figure 2.3: Change in porosity versus different vol% of Ti_3SiC_2 additions in the Al, Zn, and Sn matrix

2.4 Mechanical Performance of MRMs

The compressive strength versus displacement for the Zn-based MRM compositions can be seen in Figure 2.4. Once 30 vol% Ti_3SiC_2 was added to the Zn matrix, a brittle failure was observed. The other compositions showed a gradual failure.

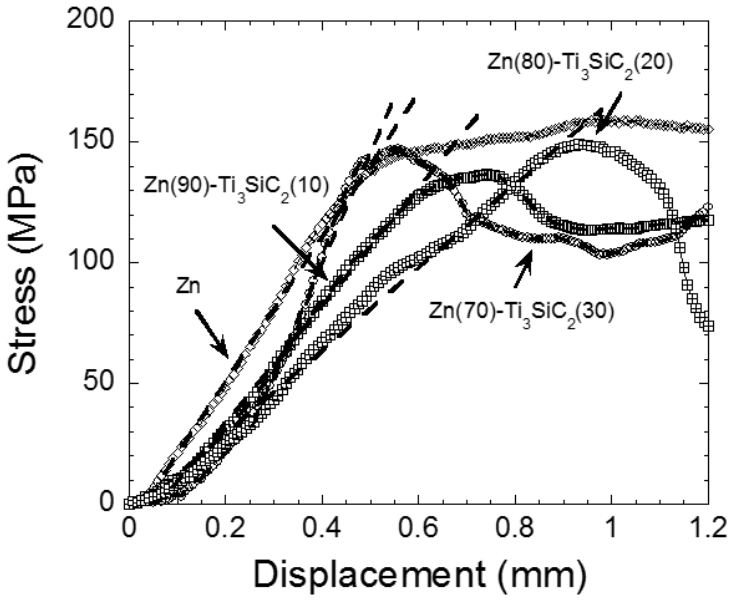

Figure 2.4: Compressive stress versus displacement profiles of different Zn matrix composites

A plot of the yield strength versus Ti_3SiC_2 additions can be seen in Figure 2.5. The yield strength did not show much of a change with the addition of Ti_3SiC_2. The addition of 5 vol% Ti_3SiC_2 had a yield strength of 120±26 MPa and the 10 vol% Ti_3SiC_2 had a yield strength of 132±19 MPa. The addition of 30 vol% Ti_3SiC_2 showed the best results with a yield strength of 147±22 MPa.

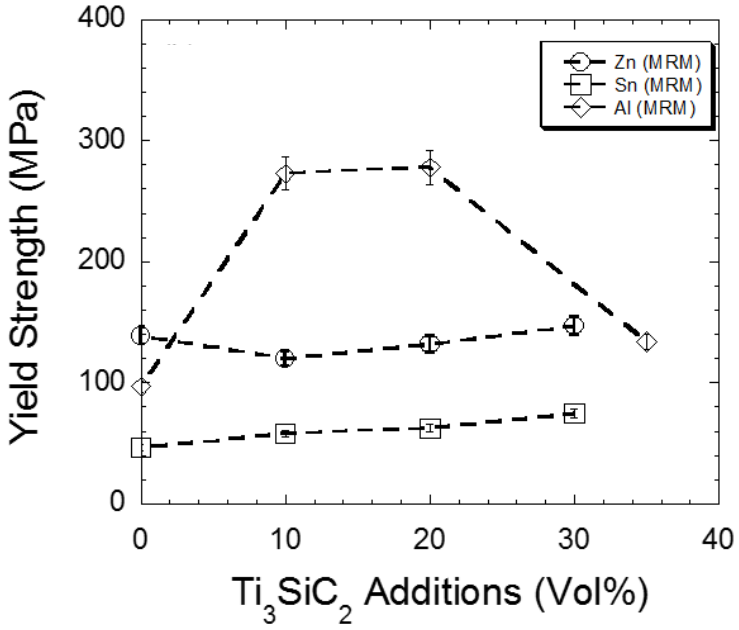

Figure 2.5: The effect of Ti_3SiC_2 additions on the yield strength of Al, Zn, and Sn matrix composites

Al-[14] and Sn-based MRMs [15] showed an increase in the yield strength unlike Zn as more Ti_3SiC_2 particulates were added to the matrices except for the 35 vol% in the Al [14]. This result decreased because of the high porosity. Brittle failure was observed in all cases as more Ti_3SiC_2 particulates were added to the matrix.

Figure 2.6 shows the hardness of the Zn-MRM composites with Sn [14] and Al [15] for comparison. The addition of 10 vol% Ti_3SiC_2 showed a slight increase in hardness, but as more Ti_3SiC_2 particulates were added, the hardness began decreasing. Al had a gradual increase with

higher additions of Ti_3SiC_2 and Sn showed little to no change as more Ti_3SiC_2 was added to the matrix [14,15].

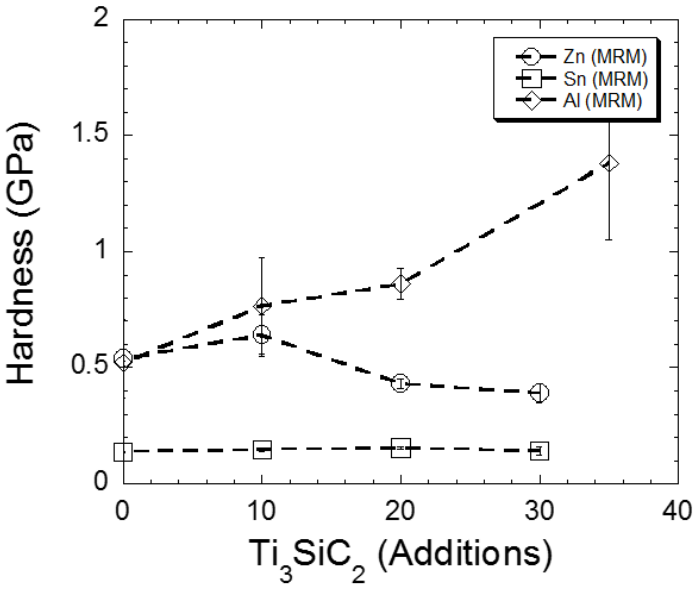

Figure 2.6: The effect of Ti_3SiC_2 additions on the hardness of Al, Zn, and Sn matrix composites

It is expected that the interaction, processing, and ductility of the metal matrix directly effects the mechanical performance of the Ti_3SiC_2 particulates within the metal matrix. For example, Zn is a hexagonal metal which causes it to be less ductile compared to Al [16]. The addition of Ti_3SiC_2 particulates has very complex interactions with different metal matrices and more fundamental studies are needed to understand these interactions.

2.5 Tribological Behavior of MRMs

Figure 2.7 shows how Ti_3SiC_2 particulates effect the tribological behavior of the Zn composites. The pure Zn showed very unstable behavior but as Ti_3SiC_2 was added to the matrix the results became much more stable.

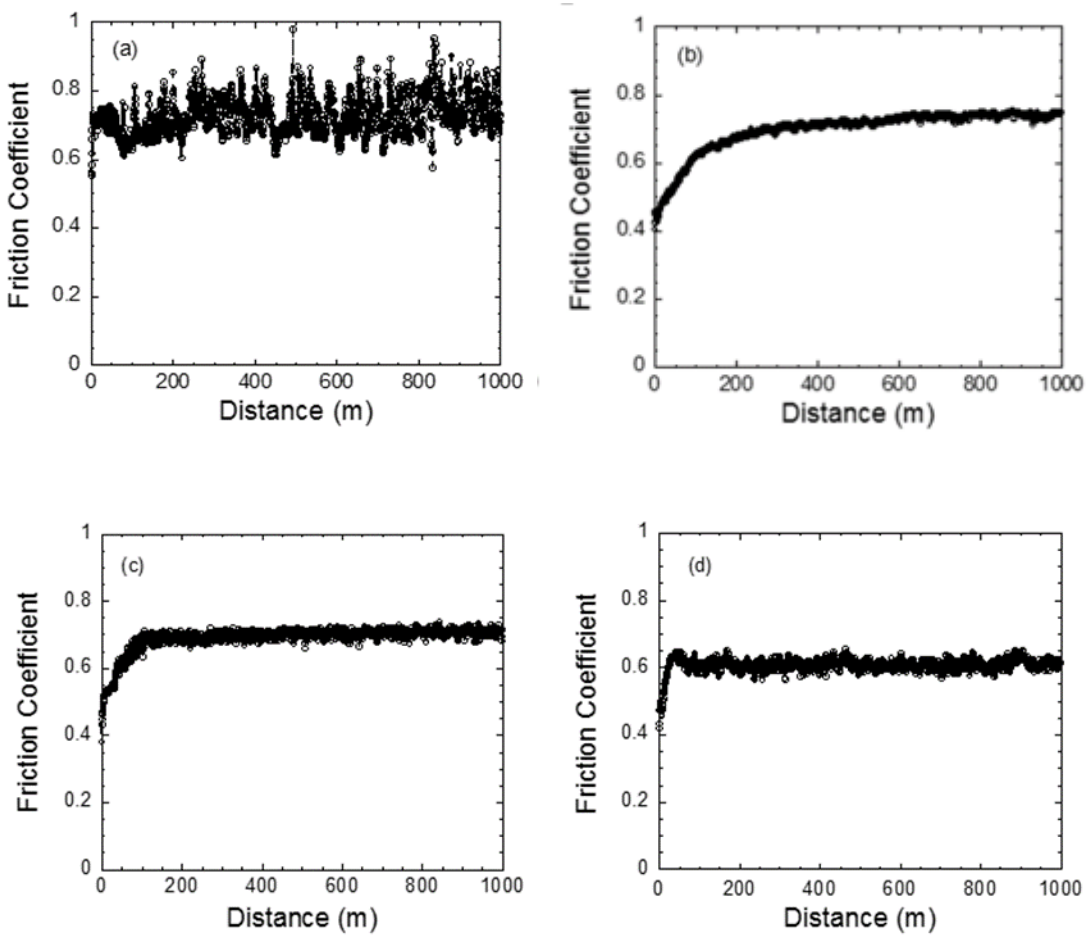

Figure 2.7: Comparison of friction coefficient (μ) versus distance profile of (a) Zn, (b) Zn(90)-Ti_3SiC_2(10), (c) Zn(80)-Ti_3SiC_2(20), and (d) Zn(70)-Ti_3SiC_2(30) against alumina substrates at RT, 5N load, and 50 cm/s rotation speed

Figure 2.8 shows a gradual decrease in the μ_{mean} as more Ti_3SiC_2 was added to the Zn matrix. Al-MRMs and Sn-MRMs showed similar results for the μ_{mean}.

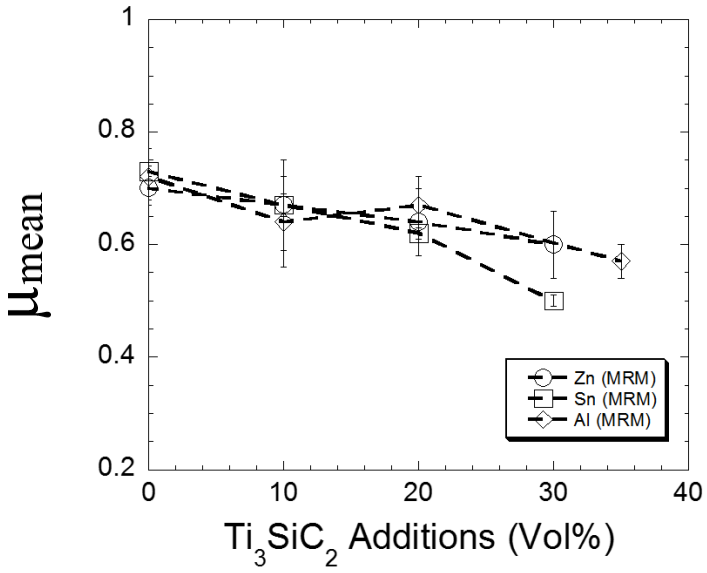

Figure 2.8: Plot of mean friction coefficient (μ_m) versus vol% of Ti_3SiC_2 additions in the Zn (MRM). For comparison, the results of Al [14] and Sn [15] based MRMs are also plotted

The WRs for the Zn-MRMs can be seen in Figure 2.9. All of the tested composites showed WRs that varied from (2-7)x10^{-4} $mm^3/N*m$ under a 5N load. Ti_3SiC_2 particulates showed a decrease in WR compared to the pure Zn, with the optimum results being at 20 vol% Ti_3SiC_2. The WR slightly increased when 30 vol% Ti_3SiC_2 was added to the matrix. This increase may be due to the brittle nature of these composites. Al and Sn showed results in this same range.

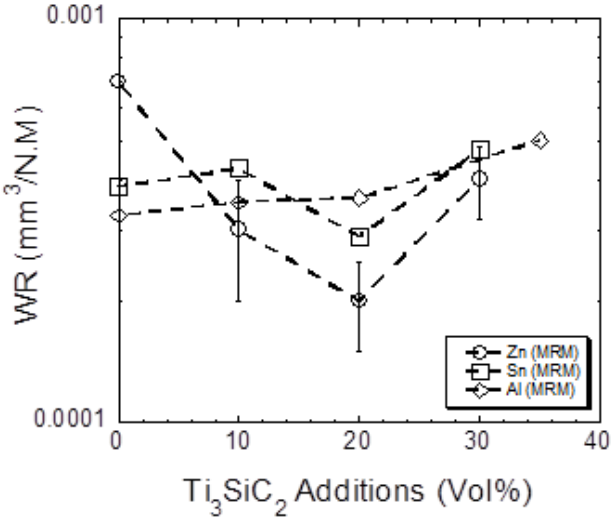

Figure 2.9: Plot of wear rate (WR) versus vol% of Ti_3SiC_2 additives in the Zn-based MRM. For comparison, the results of Al-[14] and Sn-[15] based MRMs are also plotted

SEM micrographs of the Zn(70)-Ti_3SiC_2(30) composite and the Alumina substrate were taken after tribology testing. These images are shown in Figure 2.10 (a-c). Surface wear scars can be seen on the sample in image a. Several patches of tribofilms were able to be seen on the Alumina substrate in images b-c. Mild triboxidation and wear from the Zn(70)-Ti_3SiC_2(30) to the Alumina surface caused the transfer films to form.

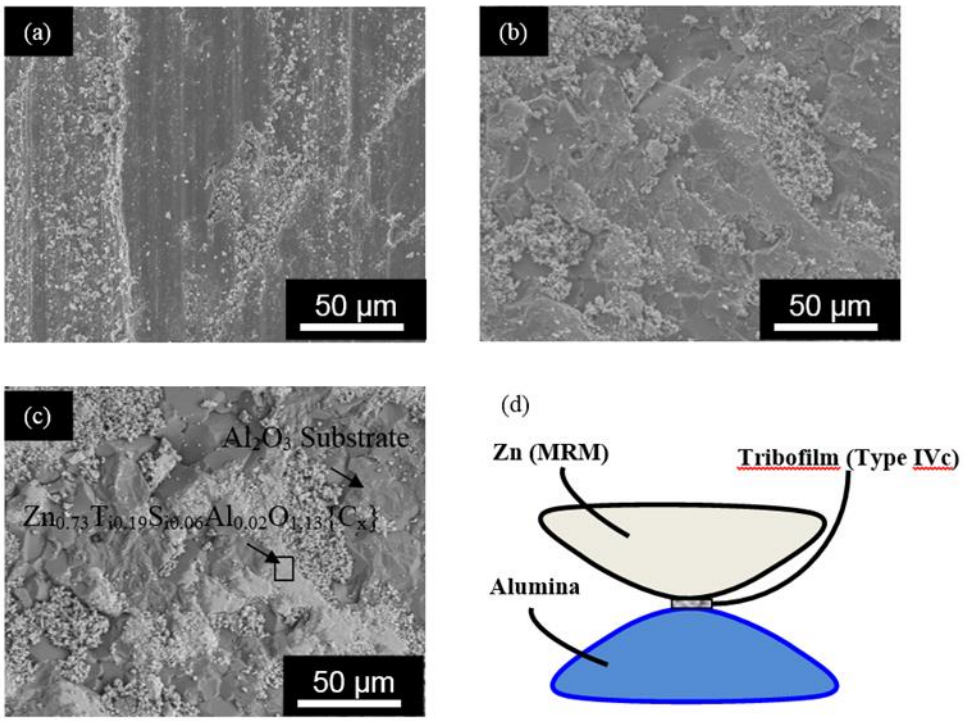

Figure 2.10: SE SEM Micrographs of (a) Zn(70)-Ti_3SiC_2(30), (b) alumina surface, and (c) BSE image of the same region, and (d) schematics of Type IVc tribofilm [14]

2.6 Tribofilm Classification

There are four categories for classifying the tribofilms according to Gupta *et al.* [8]. The categories are (a) when the source of triboreactions are from the MAX surface they are Type I, (b) when the source of triboreactions are from the counter surface they are Type II, (c) when the source of triboreactions are from both the tribopartner and the MAX phase or their composites they are

Type III, and (d) when the source of triboreactions are from the MAX phase based composites they are Type IV. There are sub-categories that divide these four categories even further by the physical appearance of the tribofilms.

The Type IVc tribofilms seen in these composites, means that MAX based composites contributed predominately to the formation of the triboreactions, and that powdery and patchy tribofilms could be seen with the naked eye.

2.7 Conclusions

The fabrication and synthesis of Ti_3SiC_2 reinforced Zn matrix composites were reported for the first time. The Zn matrix composites improved in tribological behavior with the additions of Ti_3SiC_2 during dry sliding. Zn based MRMs showed a gradual decrease in μ_{mean} from 0.70±0.02 in pure Zn to 0.60±0.06 in Zn(70)-Ti_3SiC_2(30). The tribofilms were visible with the naked eye and were patchy which classified them as Type IVc. The mechanical performance did not show any beneficial effect with the addition of Ti_3SiC_2 particulates. The metal matrix, processing parameters, and interaction of the Ti_3SiC_2 particulates with the metal matrix effected the mechanical performance.

CHAPTER III

ADDITIVE MANUFACTURING OF PHOTOPOLYMER RESIN AND Ti_3SiC_2 COMPOSITES

3.1 Introduction

Polymers and their composites have excellent friction and wear characteristics, corrosion resistance and mechanical properties [1-6]. By adding different additives [2-14], the mechanical and tribological performance of polymers can be further enhanced. As a background, $M_{n+1}AX_n$ (MAX) phases (over 60+ phases) are thermodynamically stable nanolaminates where n is 1, 2, or 3, M is an early transition metal element, A is an A-group element and X is C or N. MAX phases are layered hexagonal (space group D^4_{6h}–$P6_3/mmc$) with two formula units per cell. These solids are highly damage tolerant, thermal shock resistant, and readily machinable [15-19]. Recently it was reported that the addition of Ti_3SiC_2 particulates (MAX Phase) in both thermosets [20] and thermoplastics [21-23] can enhance the mechanical performance and solid-lubrication behavior of Polymer-MAX composites (PMCs). MAXPOL, composites of MAX phases and polymers, was used to designate this new generation of composites [19, 20].

3.2 Experimental

Clear photopolymer resin (GPCL02, Formlabs Inc., Somerville, MA) and calculated concentrations of Ti_3SiC_2 powder (-325 mesh, Kanthal, Hallstahammar, Sweden) were mixed in a ball mill (QM-5L, MTI Corporations, Richmond, CA) for 3 hours. The blends were then poured into the resin tank of the 3D printer (Form 1+, Formlabs Inc., Somerville, MA). Samples of two different geometries (tensile specimens, and cylinders) were created on PTC Creo Direct 3.0 M030

and saved as STL files. The STL files were then uploaded in a program (PreForm Software, Formlabs Inc., Somerville, MA). The tensile specimens were fabricated by following the specification in ASTM standard D638-03. The disks used for tribological study had a thickness and diameter of 3 mm and 37.5 mm, respectively. After the completion of printing, the specimens were immersed in ethyl alcohol for 10 minutes to remove any excess resin from the sample. These new generation composites will be referred to as MRPs (MAX-Reinforced Polymers) in the text as the concentration of Ti_3SiC_2 is low in the matrix, and to differentiate from MAXPOLs. MRPs were designed by adding 0.1 wt% (Resin-0.1%312Si), 0.5 wt % (Resin-0.5%312Si), 1 wt% (Resin-1%312Si), and 2 wt% Ti_3SiC_2 (Resin-2%312Si) in the resin matrix. For comparison, samples of pure resin were also fabricated by following the above-mentioned procedure.

The theoretical density of the composites was calculated from the rule of mixtures by using the theoretical density of Ti_3SiC_2 and resin. The experimental density of the composites was calculated from the mass and dimensions of each sample. The relative density was calculated by normalizing the experimental density with theoretical density. Tensile testing was conducted in a mechanical testing unit (Shimadzu AD-IS UTM, Shimadzu Scientific Instruments Inc., Columbia, MD). For each composition, a set of 5 samples was tested at a rate of 1 mm/min by using a 5 kN load cell. Stress versus displacement plots are reported as experimental limitations did not allow for accurate measurement of the actual strain during mechanical testing. In the paper, yield strength is defined as the critical stress at which the stress versus displacement plot transitions from the linear to non-linear regime. The linear region of the composites had a regression of $R^2 > 0.95$. Reported within this text is the average of 5 yield strength measurements for each composite [18]. All composites were polished ($R_a < 1\mu m$) and then tested by a Shore D hardness tester

(Durometer OS-1-E, Rex Durometers, Buffalo Grove, IL). Shore D hardness was performed by loading the samples until the reading settled. In the text, an average of five readings for each composite is reported.

Secondary Electron (SE) and Backscattered Electron (BSE) images were obtained by using a JEOL JSM-6490LV Scanning Electron Microscope (JEOL USA, Inc., Peabody, Massachusetts.). The tribological behavior of these samples was studied against a stainless steel ball by the ball on disc method (CSM Instruments SA, Peseux, Switzerland) at 2 N, 5 N, and 10 N, 50 cm/s linear speed, 1000 m sliding distance, and ~8, 10, and 12 mm track radius, respectively. The disks were polished to a ~1 µm finish. A surface profilometer (Surfcom 480A, Tokyo Seimitsu Co. Ltd., Japan) was used to confirm that all the samples had a R_a <1 µm. For every composition, three experimental studies were performed. For data analysis, an average of all the friction coefficient (µ) readings was used to calculate mean response of each experiment. Thereafter, an average of three measurements was calculated and reported in the text as μ_{mean}. The mass of the samples and substrates were measured before and after the testing by a weighing scale (Model AL204, Mettler Toledo, Columbus, OH). The specific wear rate (WR) was calculated from:

$$WR = (m_i - m_f)/(\rho * N * d) \quad 3.1)$$

where, m_i is the initial mass, m_f is the final mass, ρ is density of the composite, N is the applied load, and d is the total distance traversed by the tab during the tribology testing.

3.3 Microstructure and Phase Analysis

Figure 3.1 shows SE images of different resin-based MAX Reinforced Polymers (MRP) composites. In all the samples, the Ti_3SiC_2 particles are well-dispersed in the resin matrix.

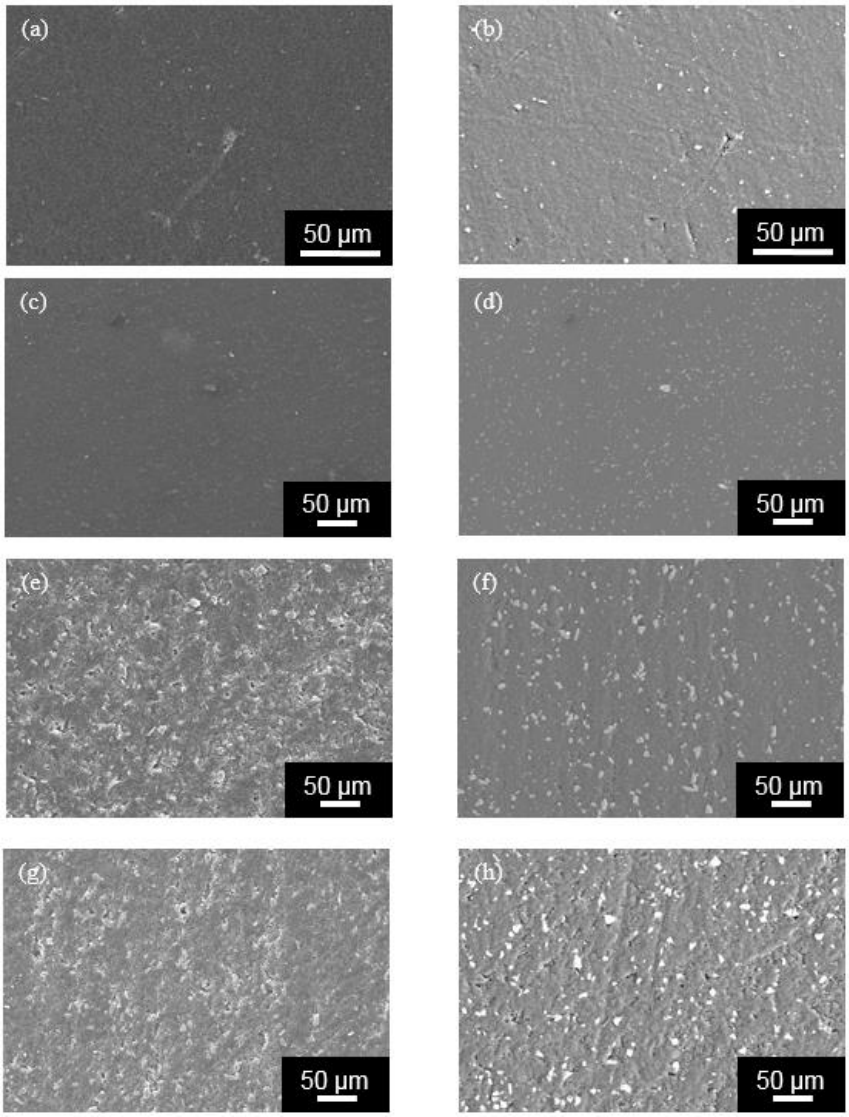

Figure 3.1: SE micrographs of Resin-0.1%312Si (a) SE and (b) BSE, Resin-0.5%312Si (c) and (d), Resin-1%312Si (e) SE and (f) BSE, and Resin-2%312Si (g) SE and (h) BSE

Figure 3.2 shows porosity and hardness of the composites as a function of Ti_3SiC_2 additions. This result shows that the addition of higher vol% of Ti_3SiC_2 concentrations made the samples more porous. Concomitantly, the hardness of the MRPs gradually decreased as the volume fraction of Ti_3SiC_2 was increased to 2 vol%.

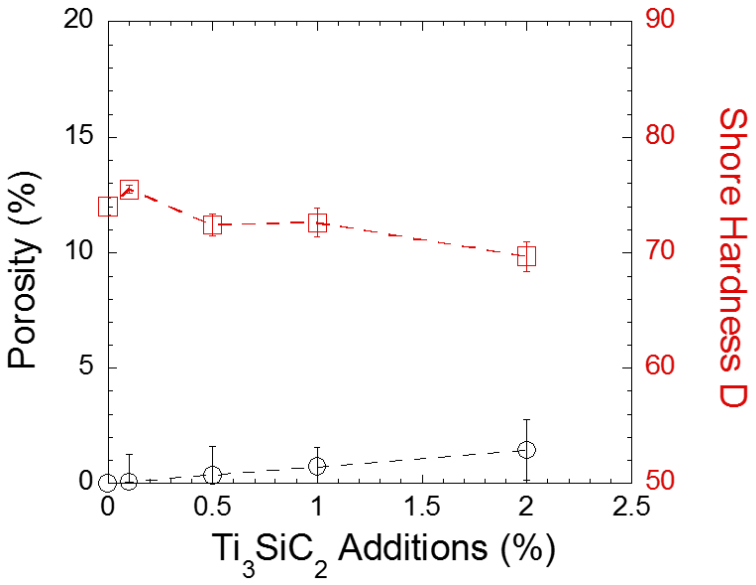

Figure 3.2: Plot of porosity (Y1) and Shore Hardness D (Y2) versus the additions of Ti_3SiC_2 particulate

3.4 Mechanical Performance of MRPs

Figure 3.3 shows the tensile stress versus displacement plots for the 3D printed pristine resin sample. The maximum stress observed during the testing is defined as ultimate tensile strength (UTS) and the stress at which the sample failed is defined as rupture strength in the text.

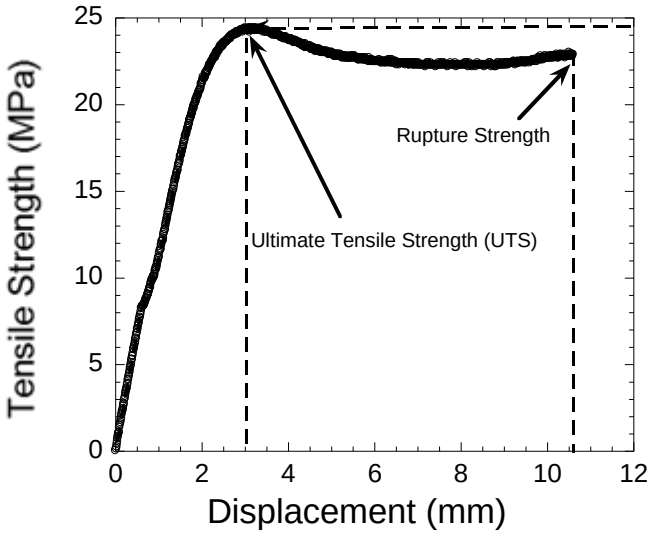

Figure 3.3: Plot of tensile strength versus displacement

Figure 3.4 shows the plot of the tensile stress versus displacement of different compositions. Figure 3.5 summarizes the UTS as function of Ti_3SiC_2 content. The 3D printed resin had a tensile strength of ~24 MPa, and the compositions retained their strength when 0.1 wt% Ti_3SiC_2 was added into the polymer matrix; however, the tensile strength gradually decreased as the concentration of Ti_3SiC_2 was increased in the matrix. At this juncture, the exact mechanisms of decrease in mechanical strength are not clear. In a separate study, Gupta *et al.* [21] had observed dewetting between UHMWPE (Ultra High Molecular Weight Polythylene) and Ti_3SiC_2 particulates. It can be hypothesized that dewetting between Ti_3SiC_2 particulates and the resin matrix and/or increase in porosity by adding higher concentration of Ti_3SiC_2 (Fig. 3.2) can cause the significant deterioration in strength. More studies are needed to understand the fundamental interaction between Ti_3SiC_2 particulates and resin matrix.

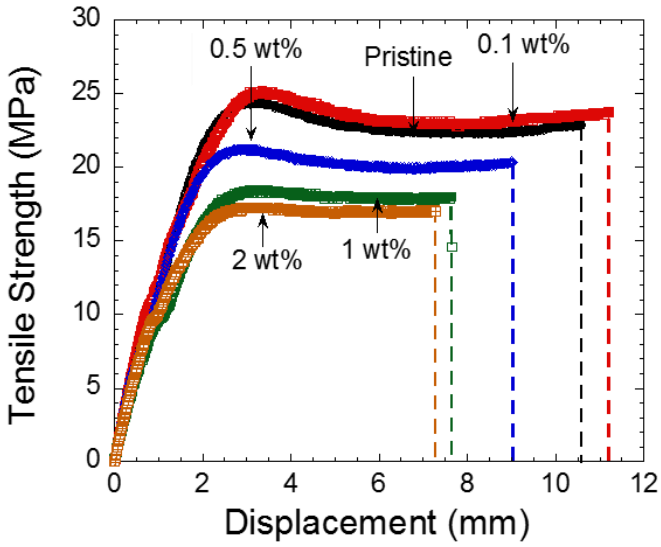

Figure 3.4: Plot of tensile strength versus displacement of different Ti_3SiC_2-resin composites

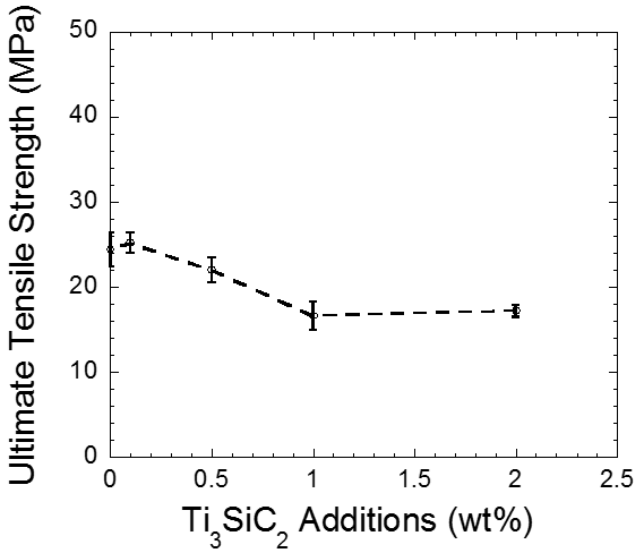

Figure 3.5: Ultimate tensile strength (UTS) of 3D printed composites as a function of Ti_3SiC_2 particulate

3.5 Tribological Performance of MRPs

Figure 3.6 shows the plot of variation of μ_{mean} as a function of Ti_3SiC_2 concentration. During testing at all loads, μ_{mean} decreased gradually as the Ti_3SiC_2 concentration was increased to a minimum in resin-1%312Si; thereafter, it gradually increased as the concentration of Ti_3SiC_2 was increased in the matrix to 2 wt%.

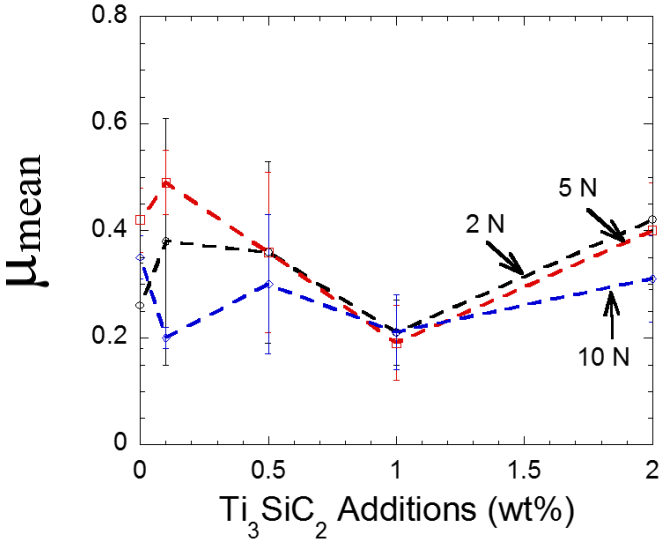

Figure 3.6: Plot of friction coefficient versus Ti_3SiC_2 additions in the resin matrix

Comparatively, Fig. 3.7 plots the WRs of all resin-based MRPs. Initially, the addition of Ti_3SiC_2 particulates gradually lowered WR until Resin-0.5%312Si, thereafter, the WRs increased as the concentration of Ti_3SiC_2 particulates was further increased. By analyzing the mechanical behavior and tribological data, it can be surmised that Ti_3SiC_2 particulates improved the tribological behavior until a critical concentration (0.5-1 wt% Ti_3SiC_2 additions); but as the tensile strength is lowered as the concentration of Ti_3SiC_2 particulates is increased in the matrix, the WRs of the composites increases as the concentration of Ti_3SiC_2 is increased in the matirx.

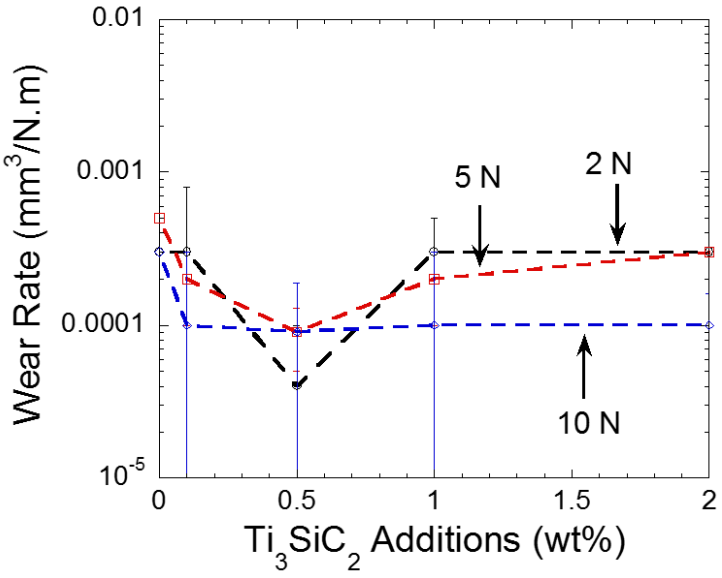

Figure 3.7: Plot of wear rate (WR) versus Ti_3SiC_2 additions

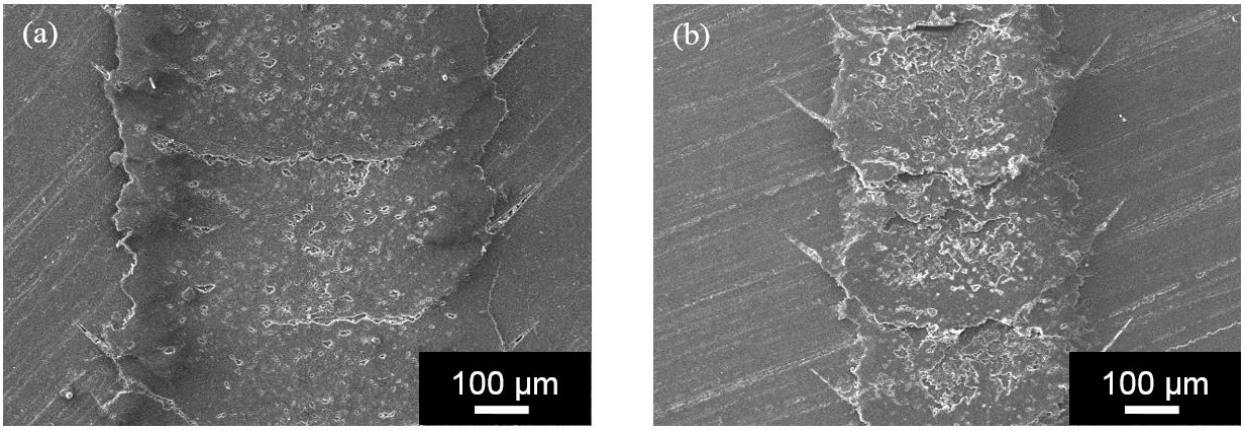

Figure 3.8: SEM SE micrograph of wear rate track of, (a) Resin and (b) Resin-0.5%312Si after testing at 5 N, 50 cm/s for 1000 m

Figure 3.8 shows the SEM micrographs of the resin and Resin-0.5%312Si after tribology testing. Comparatively, the wear scars observed on the surface of the resin are less pronounced than Resin-0.5%312Si surface. Clearly, the addition of Ti_3SiC_2 particulates decreased the adhesive wear and significantly improved the tribological performance of 3D printed samples.

3.6 Conclusion

This is the first study to report the mechanical and tribological behavior of Ti_3SiC_2 reinforced 3D printed (MRP) samples. The important conclusions of this chapter are:

1. The addition of Ti_3SiC_2 particulates decreased the UTS of MRPs.
2. The addition of Ti_3SiC_2 particulates had a beneficial effect of tribological behavior, but over a narrow range of Ti_3SiC_2 particulate concentration (0.5-1 wt% Ti_3SiC_2).
3. The addition of Ti_3SiC_2 particulates was also able to reduce adhesive wear in 3D printed components.

CHAPTER IV

ADDITIVE MANUFACTURING OF PHOTOPOLYMER RESIN AND NYLON COMPOSITES

4.1 Introduction

It is well-known that Nylon-6 (Polyamide-6) is a semi-crystalline engineering thermoplastic which has an excellent combination of strength, modulus, and chemical resistance. Nylon-6 is also used in many potential applications, for example, in automobiles, appliances, and other commercial products where properties like creep resistance, stiffness, and some toughness are required along with weight and cost savings considerations [1]. Among many types of synthetic fabrics, nylon is also one of the most widely used in various clothing products and the carpet industry [2, 3]. Nylon-based carpets are a major constituent of 4-6 million tons of carpets disposed in landfills worldwide annually [4]. Pan *et al.* [3] summarized that by reusing waste nylon carpets petro-based polymers environmental pollution can be reduced, and sustainable material industries promoted. The goal of this chapter is to understand the effect of Nylon particulates in 3D printing of resin-based systems.

4.2 Experimental

Clear photopolymer resin (FLGPCL02, Formlabs, Somerville, MA) and calculated concentrations of Nylon powder (Polyamide - Nylon 6, 15-20 µm, Goodfellow Cambridge Limited Huntingdon, England) were mixed in a ball mill (QM-5L, MTI Corporations, Richmond, CA) for 3 hours. The mixed blends were then poured into the resin tank of the 3D printer (Form 1+, Formlabs, Somerville, MA), and tensile specimens and cylinders were immediately printed. The

engineering drawings of the tensile specimen and the cylinder were created on PTC Creo Direct 3.0 M030 and saved as STL files. They were then uploaded to a program (PreForm, Formlabs, Somerville, MA). The tensile specimens were fabricated by following ASTM standard D638-03. The printed specimens were then denatured in ethyl alcohol for 10 minutes to remove any excess resin from the sample. Nylon-based composites were designed by adding 1 wt% (Resin-1%Nylon), 5 wt % (Resin-5%Nylon), 10 wt% (Resin-10%Nylon), 15 wt% (Resin-15%Nylon), and 20 wt% Nylon(Resin-20%Nylon) in the resin matrix. For comparison, a sample of pure resin was also fabricated by following the above-mentioned method

The theoretical density of the composites was calculated from the rule of mixtures by using the theoretical density of Nylon and resin phases. The experimental density of the composites was calculated from the mass and dimensions of each sample. The relative density was calculated by normalizing the experimental density with theoretical density. The composites that were printed in tensile form were tested. Tensile testing was conducted in a mechanical testing unit (Shimadzu AD-IS UTM, Shimadzu Scientific Instruments Inc., Columbia, MD). For each composition, a set of five samples were tested at a rate of 1 mm/min and a force of 50 kN. Stress versus displacement plots are reported as experimental limitations did not allow for accurate measurement of the actual strain during mechanical testing. In this paper, yield strength is defined as the critical stress at which the stress versus displacement plot transitions from the linear to non-linear regime. The linear region of the composites had a regression of $R^2 > 0.95$. Reported within this text is the average of five yield strength measurements for each composite [18]. All composites were polished ($R_a < 1\mu m$) and then tested by a Shore D hardness tester (Durometer OS-1-E, Rex

Durometers, Buffalo Grove, IL). Shore D hardness was performed by loading the samples until the reading settled. In the text, an average of five readings for each composite is reported.

Secondary Electron (SE) and Backscattered Electrons (BSE) images were obtained by using a JEOL JSM-6490LV Scanning Electron Microscope (JEOL USA, Inc., Peabody, Massachusetts.). The tribological behavior of these samples was studied against stainless steel balls by the ball on disc method (CSM Instruments SA, Peseux, Switzerland) at 5 N with a 50 cm/s linear speed, 1000 m sliding distance, and ~9 mm track radius. The disks used for the study had a thickness of 3 mm and a diameter of 37.5 mm. The disks were polished to a ~1 µm finish. A surface profilometer (Surfcom 480A, Tokyo Seimitsu Co. Ltd., Japan) was used to confirm that all the samples had a R_a <1 µm. For every composition, three experimental studies were performed. For data analysis, an average of all the friction coefficient (µ) reading was used to calculate mean response of each experiment. Thereafter, an average of three measurements was calculated and reported in the text as μ_{mean}. The mass of the samples and substrates was measured before and after the testing by a weighing scale (Model AL204, Mettler Toledo, Columbus, OH). The specific wear rate (WR) was calculated from:

$$WR = (m_i - m_f)/(\rho * N * d) \quad (4.1)$$

where, m_i is the initial mass, m_f is the final mass, ρ is density of the composite, N is the applied load, and d is the total distance traversed by the tab during the tribology testing.

4.3 Mechanical Performance of Nylon

Figure 4.1 shows the microstructure of Resin-10wt% Nylon sample. The sample is homogenous in the microscale. Figure 4.2 shows the tensile stress versus displacement plot of the 3D printed resin. Like the last chapter, the maximum stress observed during the testing is defined

as Ultimate Tensile Strength (UTS) and the stress at which the sample failed is defined as rupture strength in the text.

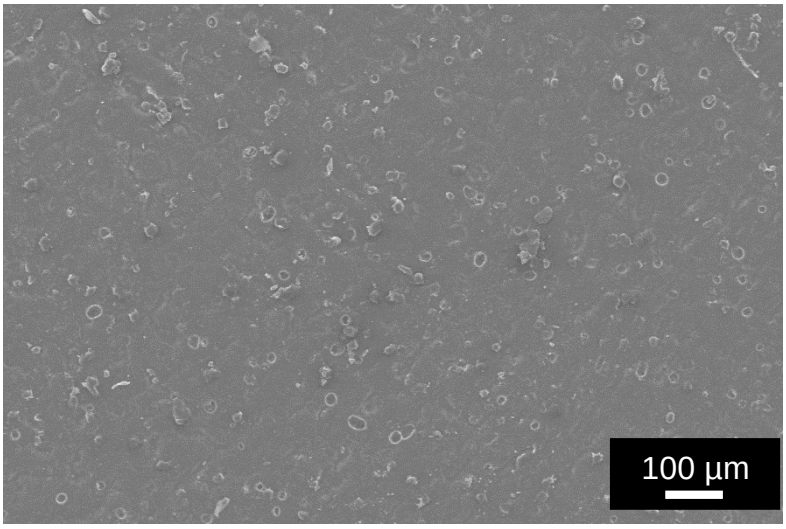

Figure 4.1: SE SEM micrographs of the microstructure of Resin-10wt% Nylon

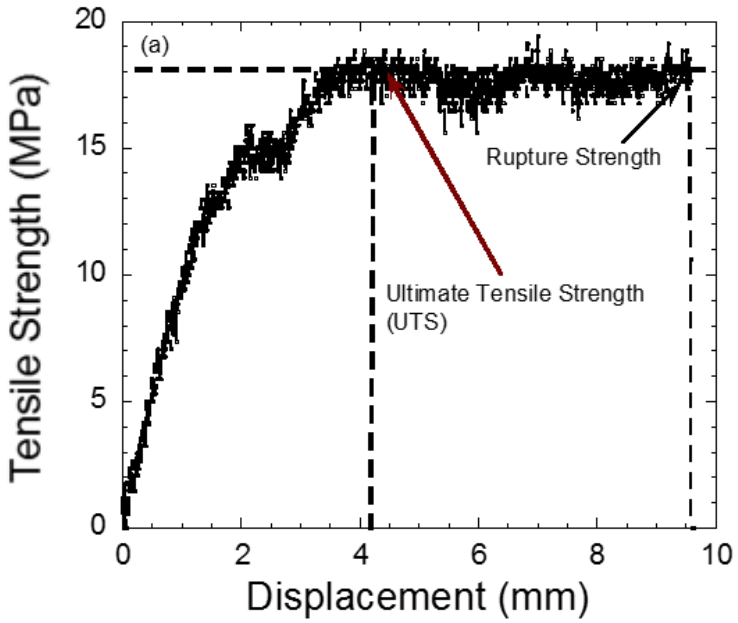

Figure 4.2: Plot of tensile strength versus displacement for 3D printed Resin

Figure 4.3 shows the comparison of the tensile strength of different Nylon-Resin samples. Fig. 4.4 plots the UTS and hardness of all the compositions. Comparatively, pure Resin had a tensile strength of ~19 MPa; however, when 5 wt% Nylon was added in the matrix, the UTS

decreased to ~9 MPa. On further additions of Nylon, the tensile strength retained similar values. All the compositions showed similar hardness values. Most probably, nylon particulates are not bonding at the molecular level with resin matrix. Further studies are needed to understand and enhance the bonding mechanisms between Nylon particulates and the resin matrix. Some of the treatments which are recommended for future studies are hot pressing, UV curing, surface modification, etc.

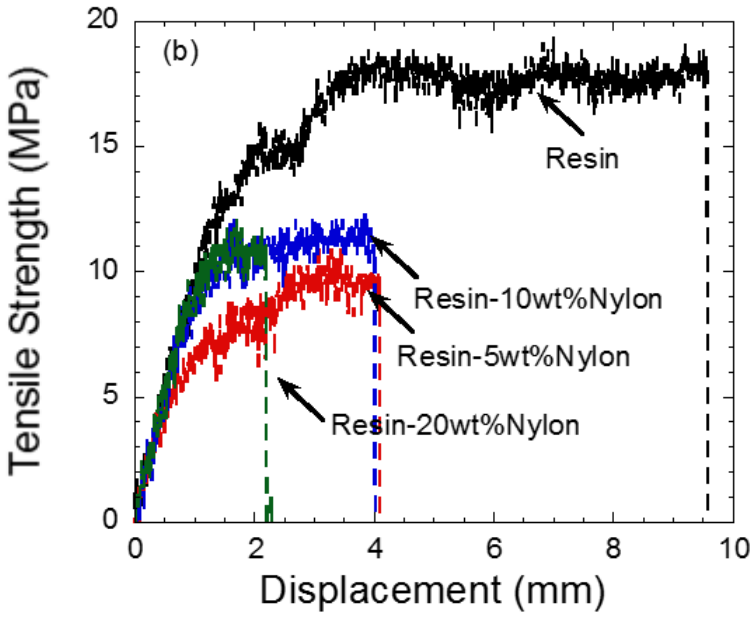

Figure 4.3: Plot of tensile strength versus displacement of different 3D printed resin-nylon samples

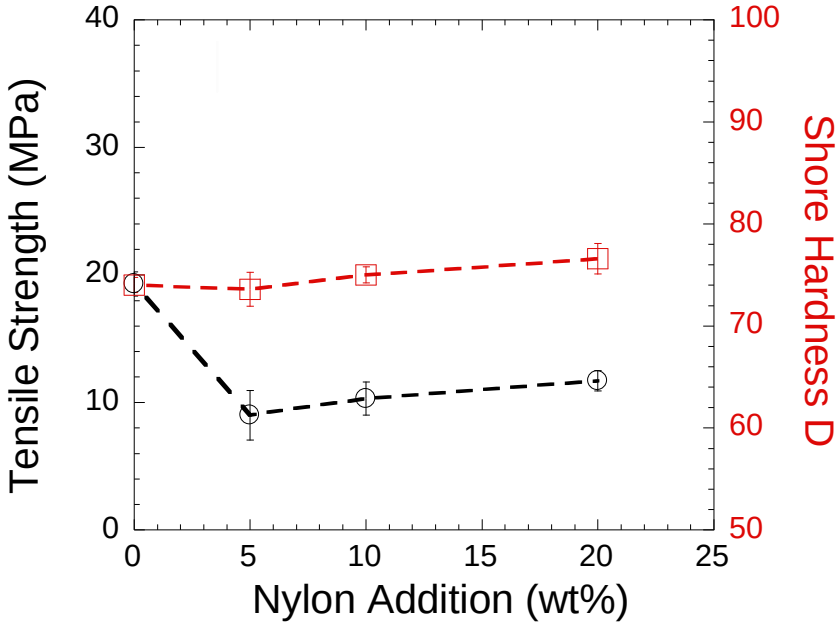

Figure 4.4: Ultimate tensile strength (Y1) and hardness (Y2) versus Nylon additions for all the designed compositions

4.4 Tribological Behavior of Nylon

Figure 4.4 shows the μ_{mean} and wear rate of Resin-Nylon samples. The μ_{mean} and WR gradually decreased as the concentration of Nylon was increased in the matrix. For example, the μ_{mean} of resin and Resin-20%Nylon were ~0.42 and ~0.10, respectively, and the concomitant WR of resin and Resin-20%Nylon were ~2.7 x 10^{-4} $mm^3/N*m$ and ~2.0 x 10^{-5} $mm^3/N*m$, respectively. In other words, the WR is improved by 13.5 times by adding 20 wt% Nylon in resin matrix. Figures 4.5 a and b show the SEM micrographs of the resin and Resin-10%Nylon after tribology testing, respectively. It is evident by examining Fig. 4.5a that the resin surface is covered with adhesive wear scars whereas the adhesive wear scars were dramatically reduced in the Resin-10%Nylon

sample. Clearly, the addition of Nylon particulates improved the tribological behavior of 3D printed samples.

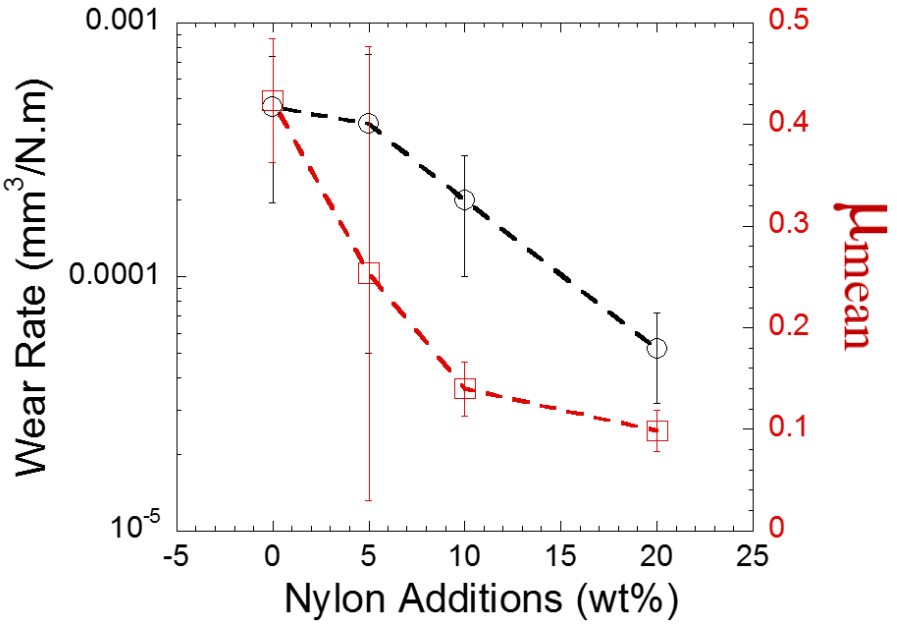

Figure 4.5: Plot of wear rate (Y1 - black) and mean friction coefficient (Y2 - red) versus Nylon additions

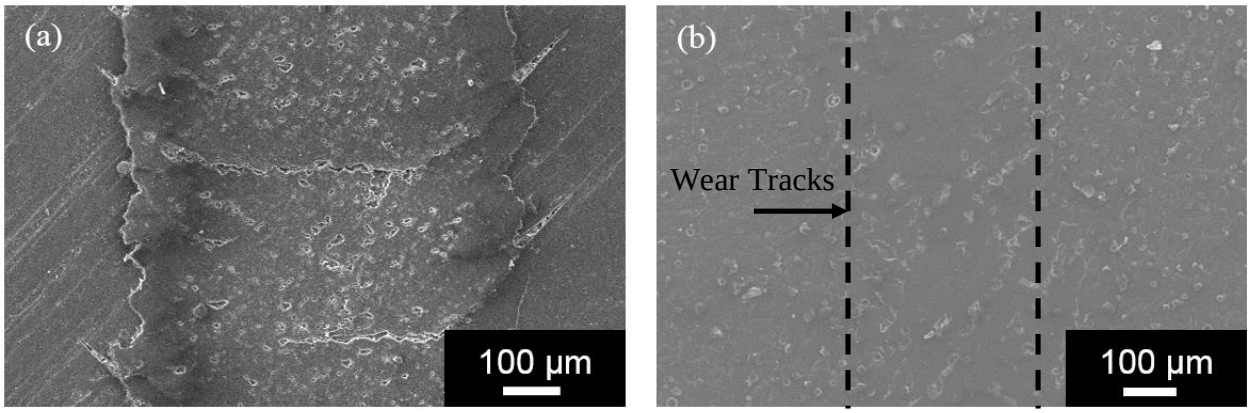

Figure 4.6: SEM SE micrograph of wear rate track of, (a) resin and (b) Resin-10%Nylon after testing at 5 N, 50 cm/s for 1000 m

4.5 Conclusions

This is the first study to document the mechanical and tribological behavior of Nylon-reinforced 3D printed resin samples. The important conclusions of this chapter are:

1. In general, the addition of Nylon particulates decreased the UTS of 3D printed samples.
2. The addition of Nylon particulates had a beneficial effect of tribological behavior.

CHAPTER V

SCOPE FOR FUTURE STUDIES

5.1 Introduction

Wind turbine blades typically consist of reinforcement fibers, such as glass fibers or carbon fibers and a plastic polymer, such as polyester or epoxy [1]. According to Anderson *et al.* [2], if the design lifetime of 20 years is assumed to be the actual lifetime of wind turbines in the future, then a rough estimate of 7.6 million tons of steel and 380,000 tons of fiber composites will have to be removed and recycled each year from 2040. Presently, these blades are recycled by (a) landfill, (b) incineration, or (c) recycling. Landfill and incineration are not viable options. The most attractive alternative is recycling, for example, material recycling, or product recycling but there are only a few established methods for the recycling of wind turbine blades [1]. In this chapter, exploratory research on recycling thermosets, more specifically, polyesters, by using them as a particulate additives in 3D printing is presented.

5.2 Experiment

Waste Polyester (POLYLITE® 413-577, Reichhold UK Ltd., Mitcham, Surrey UK) was obtained from LM Windpower, Grand Forks. The Polyester resin was crushed into powder by using a ball mill (8000 M mixer Mill, SPEX SamplePrep, Metuchen, NJ). Clear photopolymer resin (GPCL02, Formlabs Inc., Somerville, MA) and calculated concentrations of Polyester (Polyester Resin, LM Windpower, Grand Forks, North Dakota) were milled with a ball mill (QM-5L, MTI Corporations, Richmond, CA) for 3 hours. The composites were then put into the resin tank of the 3D printer (Form 1+, Formlabs Inc., Somerville, MA) and the composites were

immediately printed into tensile specimens and cylinders. The tensile specimen and the cylinder were created on PTC Creo Direct 3.0 M030 and saved as STL files. They were then uploaded to a program that came with the printer (PreForm, Formlabs, Somerville, MA). The tensile specimens were made from the ASTM standard D638-03. After printing was complete, the specimens were put into ethyl alcohol and denatured for 10 minutes to remove any excess resin from the sample. Polyester-based composites were designed by adding 5 wt% (Resin-5%Polyester), 10 wt% (Resin-10%Polyester), and 20 wt% Polyester (Resin-20%Polyester) in the resin matrix. For comparison, a sample of pure resin was also fabricated by following the above-mentioned method. Despite several attempts, any composition greater than 20 wt% Polyester addition could not be performed.

The theoretical density of the composites was calculated from the rule of mixtures by using the theoretical density of Polyester and resin phases. The experimental density of the composites was calculated from the mass and dimensions of each sample. The relative density was calculated by normalizing the experimental density with theoretical density. The composites that were printed in tensile form were tested. Tensile testing was conducted in a mechanical testing unit (Shimadzu AD-IS UTM, Shimadzu Scientific Instruments Inc., Columbia, MD). For each composition, a set of five samples were tested at a rate of 1 mm/min and a force of 50 kN. Stress versus displacement plots are reported as experimental limitations did not allow for accurate measurement of the actual strain during mechanical testing. In the paper, yield strength is defined as the critical stress at which the stress versus displacement plot transitions from the linear to non-linear regime. All composites were polished (R_a < 1µm) and then tested by a Shore D hardness tester (Durometer OS-1-E, Rex Durometers, Buffalo Grove, IL). Shore D hardness was performed

by loading the samples until the reading settled. In the text, an average of five readings for each composite is reported.

For all samples, Secondary Electron (SE) and Backscattered Electron (BSE) images were obtained by using a JEOL JSM-6490LV Scanning Electron Microscope (JEOL USA, Inc., Peabody, Massachusetts.). The tribological behavior of these samples was studied against stainless steel balls by the ball on disc method (CSM Instruments SA, Peseux, Switzerland) at 5 N with a 50 cm/s linear speed, 1000 m sliding distance, and ~10 mm track radius. The disks used for the study had a thickness of 3 mm and a diameter of 37.5 mm. The disks were polished to a ~1 µm finishing. A surface profilometer (Surfcom 480A, Tokyo Seimitsu Co. Ltd., Japan) was used to confirm that all the samples had a R_a <1 µm. For every composition, three experimental studies were performed. For data analysis, an average of all the friction coefficient (µ) reading was used to calculate mean response of a single experiment. Thereafter, average of three measurements was calculated and reported in the text as μ_{mean}. The mass of the samples and substrates were measured before and after the testing by a weighing scale (Model AL204, Mettler Toledo, Columbus, OH). The specific wear rate (WR) was calculated from:

$$WR = (m_i - m_f)/(\rho * N * d) \quad \text{----------(5.1)}$$

where, m_i is the initial mass, m_f is the final mass, ρ is density of the composite, N is the applied load, and d is the total distance traversed by the tab during the tribology testing.

5.3 Mechanical and Tribological Performance of Polyester

Figure 5.1a shows the SE SEM micrograph of the crushed nylon powders. The powdered particles are between 20-40 µm. Figure 5.1b shows the surface of 3D printed Resin-10%Polyester surface. The sample is homogenous in the microscale. Figure 5.2 shows a plot of tensile strength

of different Resin-Polyester samples. Figure 5.3 plots the UTS (Y1) and hardness (Y2) of 3D printed resin samples as a function of Polyester additions. Pure resin had a tensile strength of ~19 MPa. However, as the volume fraction of Polyester was further increased, the tensile strength decreased to ~12 MPa in Resin-5%Polyester, thereafter slightly increased to ~14 MPa in both Resin-10%Polyester and Resin-20%Polyester, respectively. The hardness of all the compositions showed similar values. Interestingly, the decrease in UTS is Resin-Polyester system was not as drastic as Ti_3SiC_2 (Chapter 3) and Nylon (Chapter 4) particulate additions. More fundamental studies to understand the interaction of Polyester particulates and Resin are recommended to further optimize the properties of these novel solids.

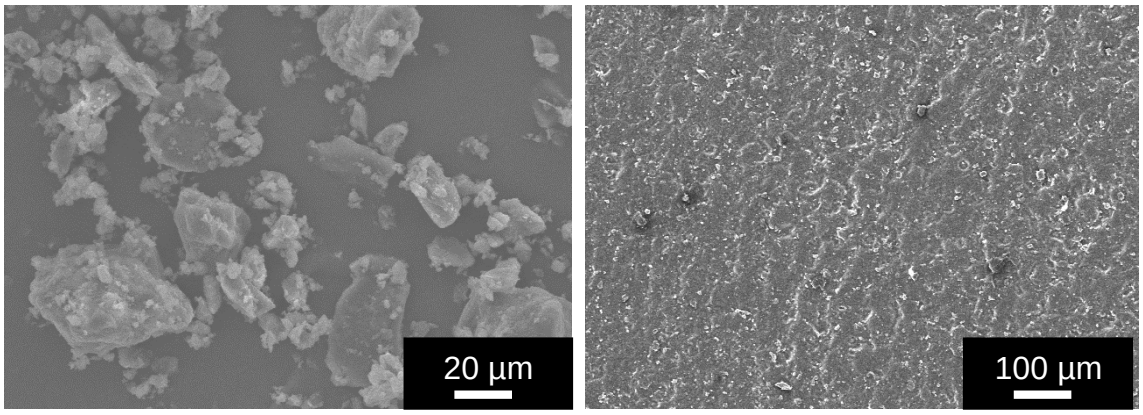

Figure 5.1: SE SEM micrographs of the (a) milled polyester powders and (b) as-printed Resin-10%Polyester surface

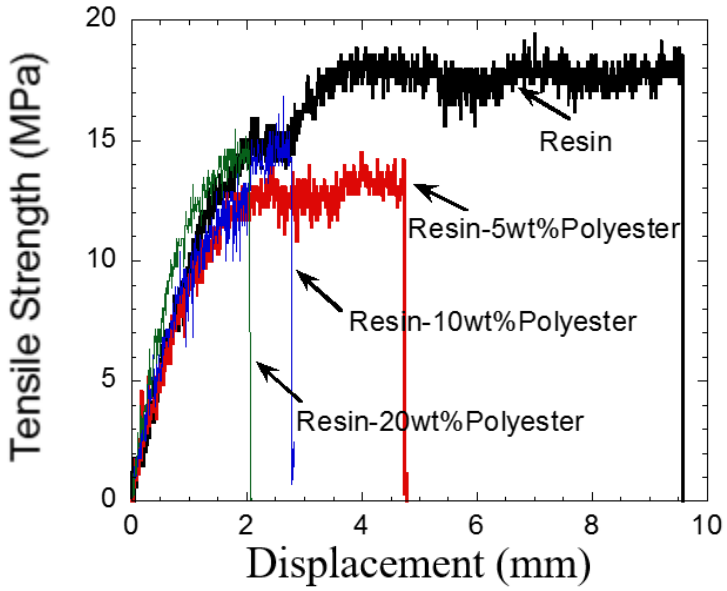

Figure 5.2: Plot of Tensile Strength versus displacement of different Resin-Polyester composites

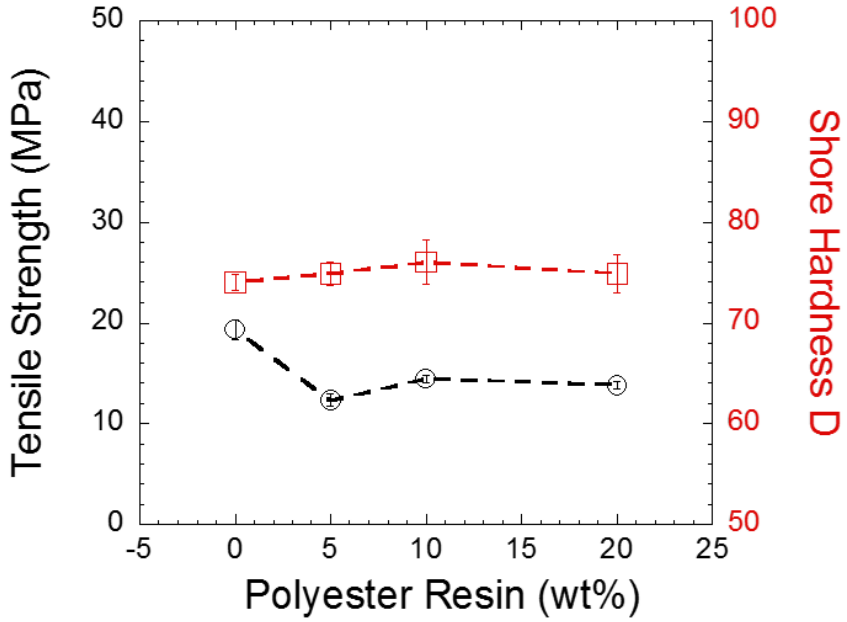

Figure 5.3: Plot of tensile strength (Y1) and Shore Hardness D (Y2) versus Polyester particulate additions

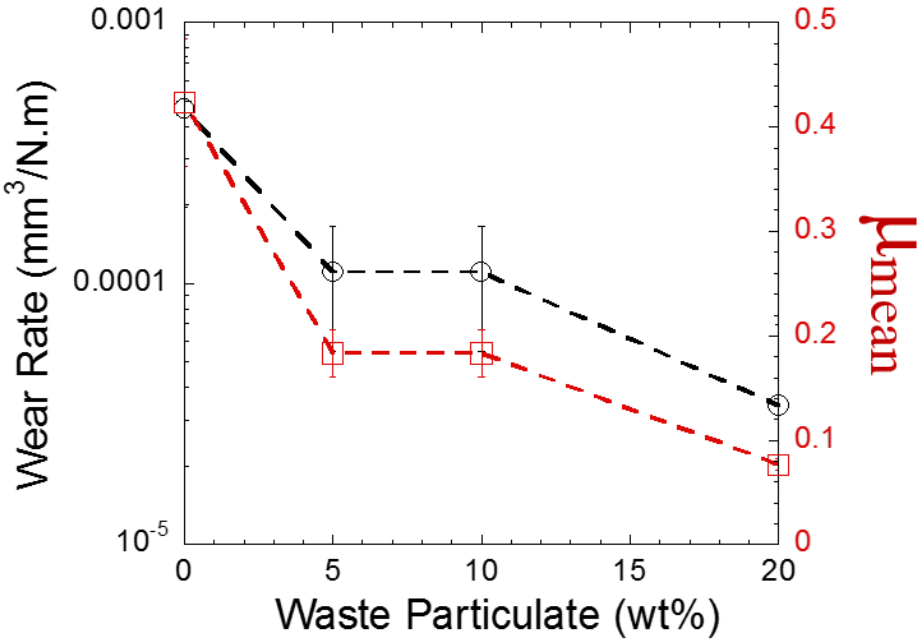

Figure 5.4: Plot of wear rate (Y1) and friction coefficient (Y2) versus Polyester additions

Figure 5.4 shows the variation of WR and μ_{mean} as a function of addition of Polyester particulates. The addition of Polyester particulates decreased the WR and μ_{mean} remarkably. The Resin-20%Polyester showed the lowest WR and μ_{mean}, for example, as compared to 3D printed resin; the WR decreased by one order of magnitude (13 times reduction) and μ_{mean} decreased significantly from ~0.42 to ~0.08, respectively. This behavior is very similar to the behavior of Nylon-Resin composites (Chapter 4), and significantly better than Ti_3SiC_2-Resin composites. It is evident by examining Fig. 5.5 that adhesive wear scars are present on the surface of the Resin. The adhesive wear scars on Resin-10%Nylon surface are barely visible (Fig. 5.5b). These results clearly demonstrate that the addition of Polyester particulates reduces adhesive wear and increases the potential of 3D printed materials for tribological purposes.

Increasingly, polymer gears are being used as they have inherent advantages like reduction in weight, solid lubrication, smooth function, resistance to corrosion, etc. Moreover, these unique

advantages have led to their integration into various low power systems [3]. These gears are used in several applications including automobiles, office machines and the food industry. Clearly, the development of novel 3D printed triboactive materials will add further impetus to the field. Moreover, if waste polymers are used in the process to further functionalize then process, then it will make the field of additive manufacturing of engineering plastics more attractive for further commercialization and research.

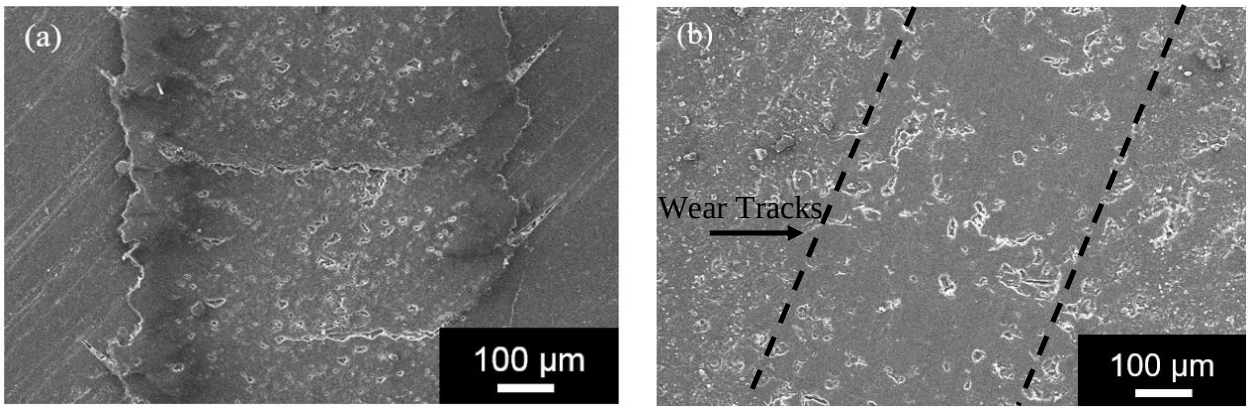

Figure 5.5: SEM SE micrograph of wear rate track of (a) resin and (b) Resin-10%Polyester after testing at 5 N, 50 cm/s for 1000 m

5.4 Conclusions

This is the first study to document the mechanical and tribological behavior of waste Polyester reinforced 3D printed resin samples. The important conclusions of this chapter are:

1. In general, the addition of Polyester particulates decreased the UTSs of 3D printed samples, but the decrease in strength was less drastic as compared to Ti_3SiC_2-Resin and Nylon-Ti_3SiC_2 composites.
2. The addition of Polyester particulates had a beneficial effect of tribological behavior. For example, as compared to 3D printed resin, the WRs decreased by one order of magnitude (13

times reduction) and μ_{mean} decreased significantly from ~0.42 to ~0.08 (5 times reduction), respectively in Resin-20%Polyester.

APPENDIX

Status of Journal Publications

1. "Synthesis and Tribological Behavior of 3D Printed Ti_3SiC_2 Reinforced Polymer Matrix Composites", (to be submitted)

2. "MAXPOL: Novel Solid-Lubricant Materials for Multifunctional Applications", Journal of Plastics Research Online

3. "On the Synthesis and Tribological Behavior of PEEK-Ti_3SiC_2 Composites during Self-Mating", Applied Composite Materials

4. "Synthesis and Characterization of Ti_3SiC_2 Particulate-Reinforced Novel Zn Matrix Composites", Journal of Materials Engineering and Performance, 24, 4071-4076 (2015)

Contributed Presentations During Master's Degree

1. "3D Printing of MAX Reinforced Composites", R. Dunnigan, S. Gupta, Department of Mechanical Engineering, Grand Forks, North Dakota

2. "Novel MAX-Metal and MAX-Polymer Multifunctional Composites", R. Dunnigan, S. Ghosh, M.A. Habib, S. Gupta, Department of Mechanical Engineering, Grand Forks, North Dakota

3. "Novel Metal Matrix Multifunctional Materials by Ti_3SiC_2 Reinforcements", R. Dunnigan, M.A. Habib, S. Ghosh, S. Gupta, Department of Mechanical Engineering, Grand Forks, North Dakota

4. "Tribology of MAX Phase Reinforced Novel Soft Metal Composites", R. Dunnigan, S. Gupta, 2015 Scholarly Forum, Grand Forks, North Dakota

5. "Novel MAX-polymer Multifunctional Composites", S. Ghosh, R. Dunnigan, M. Habib, S. Gupta, ICACC 2016, Daytona Beach, Florida.

6. "On the Development of MAX Reinforced Metal Matrix Composites", M. Habib, R. Dunnigan, S. Ghosh, S. Gupta, ICACC 2016, Daytona Beach, Florida.

7. “Development of Novel Additive Manufacturing (AM) Practices”, R. Dunnigan, S. Ghosh, M. Habib, S. Gupta, ICACC 2016, Daytona Beach, Florida.

8. “Tribology of Polymer Matrix Composites (PMCs) Fabricated by Additive Manufacturing”, S. Gupta, R. Dunnigan, A. Salem, L. Kuentz, M. C. Halbig, M. Singh, ICACC 2016, Daytona Beach, Florida.

9. “Novel Metal Matrix Multifunctional Materials by Ti_3SiC_2 Reinforcements”, Md. Ahsan Habib, R. Dunnigan, S. Ghosh, S. Gupta, MS&T 2015, Columbus, Ohio.

10. “Design of Novel Green Manufacturing Technologies”, S. Gupta, M. F. Riyad, R. Dunnigan, MS&T 2015, Columbus, Ohio.

11. “Novel MAX Phase Reinforced Soft Metal Composites”, S Ghosh, R. Dunnigan, Md. Ahsan Habib, S. Gupta, MS&T 2015, Columbus, Ohio.

12. “Manufacturing of Novel MAX-Polymer (MAXPOL) Multifunctional Composites”, R. Dunnigan, M. F. Riyad, S. Gupta, Material Science and Technology (MS&T) 2015, Columbus, Ohio.

13. “On the Development of Novel MRM (MAX Reinforced Metal) Multifunctional Materials”, S. Gupta, R. Dunnigan, 11th International Conference on Ceramic Materials and Components (ICACC) for Energy and Environmental Applications, Vancouver, June 14-19, 2015.

14. “Tribology of MAX Phase Reinforced Novel Soft Metal Composites”, R. Dunnigan, S. Gupta, T. Hammann, 2015 Society of Tribology and Lubrication Engineers (STLE) Annual Meeting and Exhibition, Dallas, Texas, 2015

REFERENCES

Chapter I

1. "A Review of Additive Manufacturing", Kaufui V.Wong and Aldo Hernandez ISRN Mechanical Engineering Volume 2012, Article ID 208760, 10 pages (2012)
2. "Rapid Prototyping: Principles and Applications", Noorani, Rafiq. Hoboken, NJ: Wiley, 2006. Print.
3. "Material increases manufacturing by rapid prototyping techniques", P. P. Kruth, CIRP Annals—Manufacturing Technology, vol. 40, no. 2, pp. 603–614, 1991.
4. "Development of Novel Max Phase Composites', T. Hammann, UMI Dissertation Publishing, 2014
5. "Research." In Materials. Drexel University, n.d. Web. 10 Jan. 2013.
6. "The MAX phases: unique new carbide and nitride materials", M.W. Barsoum, T. El-Raghy **89**, 336–45 (2000). DOI: 10.1511/2001.4.334
7. "Three-Dimensional Printing of Layered Machinable Ductile Carbide", D. J. D'Costa, S.D. Dimovski, F. Lin, T. El-Raghy, M.W. Barsoum, W. Sun, Proceedings of Eleventh Solid Freeform Fabrication Symposium, University of Texas, Austin, TX, Aug. 7-9, 2000; 12 pages.

Chapter II

1. "Damage assessment of titania filled zinc–aluminum alloy metal matrix composites in erosive environment: A comparative study", A. Patnaik, T.G. Mamatha, S. Biswas, P. Kumar, Materials and Design 36 (2012) 511–521.
2. "Dry sliding friction and wear behaviour of short fiber reinforced zinc-based alloy Composites", S. Yu, Z. He, K. Chen, Wear 198 (1996) 108-114.
3. "Dry sliding wear of garnet reinforced zinc/aluminium metal matrix composites", G. Ranganath, S.C. Sharma, M. Krishna, Wear 251 (2001) 1408–1413.
4. "Dry sliding wear of short glass fibre reinforced zinc–aluminium composites", Tribology International 31, 183–188 (1998).

5. "Investigation into sliding wear performance of zinc-based alloy reinforced with SiC particles in dry and lubricated conditions", B.K. Prasad, Wear 262 (2007) 262–273.

6. "Sliding wear response of a zinc-based alloy and its composite and comparison with a gray cast iron: influence of external lubrication and microstructural features", B.K. Prasad, Materials Science and Engineering A 392 (2005) 427–439.

7. "Cu/Ti3SiC2 composite: a new electrofriction material", Y. Zhang, Z.M. Sun, Y.C. Zhou, Mater. Res. Innov. 3, 80–84 (1999).

8. "On the tribology of the MAX phases and their composites during dry sliding: A review", S. Gupta and M.W. Barsoum, Wear 271, 1878– 1894 (2011).

9. "Ta2AlC and Cr2AlC Ag-based composites - New solid lubricant materials for use over a wide temperature range against Ni-based superalloys and alumina", S. Gupta, D. Filimonov, T. Palanisamy, T. El-Raghy and M. W. Barsoum, Wear 262, 1479-1489 (2007).

10. "Nanocrystalline M-matrix composites with ultrahigh damping properties", B. Anasori, S. Amini, V. Presser, and M. W. Barsoum, Magnesium Technology, John Wiley and Sons, Inc, 463-468 (2011).

11. "Powder metallurgy processing and compressive properties of Ti3AlC2/Al composites", W.J. Wang, V. Gauthier-Brunet, G.P. Bei, G. Laplanche, J. Bonneville, A. Joulain, S. Dubois, Mater. Sci. Eng. A 530, 168–173 (2011).

12. "Current-activated, pressure-assisted infiltration: a novel, versatile route for producing interpenetrating ceramic–metal composites", L. Hu, A. Kothalkar, M. O'Neil, I. Karaman, M. Radovic, Mater. Res. Lett. (2014), http://dx.doi.org/10.1080/21663831.2013.873498

13. "Thermo-mechanical response and damping behavior of shape memory alloy/MAX phase composites", A. Kothalkar, R. Benitez, L. Hu, M. Radovic, I. Karaman, Metall. Mater. Trans. A. 45, 2646–2658 (2014).

14. "Synthesis and Characterization of Novel Al-Matrix Composites Reinforced with Ti3SiC2 Particulates", S. Gupta, T. Hammann, R. Johnson, and M.F. Riyad, Journal of Materials Engineering and Performance, 24, 1011-1017 (2014).

15. "Novel Ti3SiC2 reinforced Sn matrix composites", T. Hammann, R. Johnson, M. F. Riyad, and S. Gupta, Proceedings of 39th Int'l Conf & Expo on Advanced Ceramics & Composites (ICACC 2015).

16. "Engineering Materials: properties and selection", K. G. Budinski, M. K. Budinsky, 9th Edition, Pearson Prentice Hall (2013).

Chapter III

1. Wang, Y.Q., Li, J. (1999), "Sliding wear behavior and mechanism of ultra-high molecular weight polyethylene", Materials Science and Engineering **A266**, pp. 155–160.

2. Guofang, G. , Huayong, Y., Xin, F. (2004), "Tribological properties of kaolin filled UHMWPE composites in unlubricated sliding", Wear **256**, 88–94.

3. Pettarin, V., Churruca, M. J., Felhos, D., Karger-Kocsis, J., Frontini, P. M. (2010), "Changes in tribological performance of high molecular weight high density polyethylene induced by the addition of molybdenum disulphide particles," Wear **269**, pp. 31–45.

4. Zhang, S. W. (1998), "State-of-the-art of polymer tribology", Tribology International **31**, pp. 49–60.

5. Xue, Y., Wu, W., Jacobs, O., Schadel, B. (2006), "Tribological behaviour of UHMWPE/HDPE blends reinforced with multi-wall carbon nanotubes", Polymer Testing **25**, pp. 221–229.

6. Panin, C.V., Kornienko, L.A., Nguyen, S. T., Ivanova, L.R., Poltaranin, M.A (2015), "The effect of adding calcium stearate on wear-resistance of ultra-high molecular weight polyethylene", Procedia Engineering **113**, pp. 490 – 498.

7. Difallah, B. B., Kharrat, M., Dammak, M., and Monteil, G. (2014), "Improvement in the Tribological Performance of Polycarbonate via the Incorporation of Molybdenum Disulfide Particles," Tribol. Trans., **57**, pp. 806-813.

8. Suñera S., Bladen C. L., Gowland N., Tipper J. L., Emam N. (2014), "Investigation of wear and wear particles from a UHMWPE/ multi-walled carbon nanotube nanocomposite for total joint replacements" Wear **317**, pp.163–169.

9. Liu Y., Sinha S. K. (2013), "Wear performances and wear mechanism study of bulk UHMWPE composites with nacre and CNT fillers and PFPE overcoat", Wear **300**, pp. 44–54.

10. Tong, J., Ma Y., Jiang M. (2003), "Effects of the wollastonite fiber modification on the sliding wear behavior of the UHMWPE composites", Wear **255**, pp.1–6.

11. 734–741.Chang , L., and Friedrich, K. (2010), "Enhancement effect of nanoparticles on

the sliding wear of short fiber-reinforced polymer composites: A critical discussion of wear mechanisms", , Tribology International **43**, pp. 2355–2364.

12. Burroughs, B. R., Kim, J-H and Blanchet, T. A. (1999), "Boric Acid Self-Lubrication of B_2O_3-Filled Polymer Composites," Tribol. Trans., **42**, pp. 592-600.

13. Jia, Z. and Yanga, Y. (2012), "Self-lubricating properties of PTFE/serpentine nanocomposite against steel at different loads and sliding velocities," Composites: Part B **43**, pp. 2072–2078.

14. Felhos D., Karger-Kocsis J., Xu D. (2008), "Tribological testing of peroxide cured HNBR with different MWCNT and silica contents under dry sliding and rolling conditions against steel," Journal of Applied Polymer Science **108**, pp. 2840–2851.

15. Barsoum, M.W. and Radovic, M, (2011), "Elastic and Mechanical Properties of the MAX Phases," Annu. Rev. Mater. Res. **41**, pp. 195-227.

16. Barsoum, M.W. and El-Raghy, T. (1996), "Synthesis and characterization of a remarkable ceramic: Ti_3SiC_2," J. Am. Ceram. Soc. **79**, pp. 1953–1956.

17. Barsoum, M.W. (2000), "The $M_{n+1}AX_n$ phases: a new class of solids; thermodynamically stable nanolaminates," Prog. Solid State Chem. **28**, pp. 201–281.

18. Amini, S., Barsoum, M.W., and El-Raghy, T. (2007), "Synthesis and mechanical properties of fully dense Ti_2SC", J. Am. Ceram. Soc. **90** (12), pp. 3953–3958.

19. Gupta, S. and Barsoum, M.W. (2011), "On the tribology of the MAX phases and their composites during dry sliding: A review," Wear **271**, pp. 1878– 1894.

20. Gupta, S., Hammann T., Johnson R., and Riyad M. F., (2015) Tribological Behavior of Novel Ti_3SiC_2 (Natural Nanolaminates)-Reinforced Epoxy Composites during Dry Sliding, Tribology Transactions, **58**, pp 560-566, DOI: 10.1080/10402004.2014.996308.

21. Gupta, S. and Riyad, M.F., (2016) Synthesis and tribological behavior of novel UHMWPE-Ti_3SiC_2 composites. Polym Compos. doi: 10.1002/pc.23925

22. "Synthesis and Tribological Behavior of Novel Wear Resistant PEEK-Ti_3SiC_2 composites" Journal of Engineering Tribology (Accepted for Publication).

23. "Novel Self Lubricating Teflon-Ti_3SiC_2 composites" To be submitted.

24. Scholes, S.C., Unsworth, A. (2010), "The wear performance of PEEK-OPTIMA based self-mating couples", Wear **268**, pp. 380–387.

CHAPTER IV

1. "Effect of SiO_2 nanoparticle on thermal and tensile behavior of nylon-6", M. M. Hasan, Y. Zhou, H. Mahfuz, S. Jeelani, Materials Science and Engineering A **429**, 181–188 (2006).

2. "Recycling of waste nylon 6/spandex blended fabrics by melt processing", F. Lv, D. Yao, Y. Wang, C. Wang, P. Zhu, Y. Hong, Composites Part B 77 (2015) 232-237.

3. "Compression molded composites from discarded nylon 6/nylon 6,6 carpets for sustainable industries", G. Pan, Y. Zhao, H. Xu, X. Hou, Y. Yang, Journal of Cleaner Production **117**, 212-220 (2016).

4. "Review: recycling of nylon from carpet waste". C. Mihut, D.K. Captain, F. Gadala-Maria, M.D. Amiridis, Polym. Eng. Sci. 41 (9), 1457-1470 (2001).

CHAPTER V

1. Larsen, K. (2009, January 31). Recycling wind. Retrieved April 23, 2016, from http://www.materialstoday.com/composite-applications/features/recycling-wind/

2. "Managing long-term environmental aspects of wind turbines: A prospective case study", Per Dannemand Andersen, M Borup, T Krogh, Int. J. Technol. Policy Manag., **7**, 339-354 (2007).

3. "A new experimental approach for measuring thermal behaviour in the case of nylon 6/6 cylindrical gears", E. Letzelter, M. Guingand, J. Vaujany, P. Schlosser, Polymer Testing **29,** 1041–1051 (2010).